Energy Reviews 5 (2026) 100193

Contents lists available at ScienceDirect

Energy Reviews

journal homepage: www.journals.elsevier.com/energy-reviews

Full Review Article

Recent advances in the application of high-entropy materials in lithium-based anodes

Shida Yang, Pengjie Ren, Wenqing Ruan *, Jiang Ma **

State Key Laboratory of Radio Frequency Heterogeneous Integration, College of Mechatronics and Control Engineering, Shenzhen University, Shenzhen, 518060, China

ARTICLE INFO

Keywords:
High-entropy
Lithium-ion batteries
Lithium storage mechanism

ABSTRACT

Lithium-ion batteries constitute the cornerstone of modern energy storage. However, commercial graphite anodes are increasingly limited by their theoretical capacity and energy density. Although high-capacity alternatives such as silicon and transition metal oxides have been explored, their practical implementation remains severely bottlenecked by structural instability. High-entropy materials (HEMs) have emerged as promising candidates capable of transcending these conventional limitations. Governed by the four fundamental core effects, HEMs exhibit unique synergistic attributes, including enhanced lattice resilience and superior electrochemical kinetics, that surpass those of conventional binary or ternary counterparts. This review systematically evaluates recent progress in HEM-based anodes for lithium storage, categorizing high-entropy alloys, oxides, and burgeoning derivatives, including sulfides and phosphides. We further dissect the multifaceted storage mechanisms and the practical hurdles facing the predominant high-entropy oxide anodes. Finally, we offer forward-looking perspectives on the field, emphasizing the integration of artificial intelligence (AI) for accelerated material discovery and the pathways toward industrial-scale application.

1. Introduction

Lithium-ion batteries (LIBs) serve as the cornerstone of electrochemical energy storage, driving the rapid proliferation of portable electronics, electric vehicles, and grid-scale renewable energy systems. As the global community transitions toward a low-carbon economy, there is an urgent demand for next-generation LIBs that break through current bottlenecks in energy density, cycling longevity, and safety. However, the intrinsic limitations of conventional electrode materials increasingly stymie commercial LIB performance [1–4].

The anode, a critical component in determining overall battery capacity and stability, remains a focal point for innovation. Although commercial graphite remains the industry standard for its stability and acceptable cost, its theoretical specific capacity cannot meet the demands of high-energy applications [5,6]. To address this, researchers have explored high-capacity alternatives, including alloy-type elements (e.g., Si, Ge, Sn) [7–11] and conversion-type transition metal oxides (TMOs) [12,13]. Although these materials offer significantly higher theoretical capacities, their practical adoption remains severely bottlenecked by massive volume expansion, structural pulverization, and poor electronic conductivity [14–16].

In response to these challenges, HEMs are being rigorously investigated as promising candidates for anode materials [17,18]. Departing from conventional systems based on a single host or binary components, HEMs integrate five or more primary constituents into a unified solid-solution phase. Applied first to high-entropy alloys (HEAs) in 2004 [19], the high-entropy strategy was later extended to oxides in 2015 [20]. The validation of high-entropy oxides (HEOs) as LIB anodes was pioneered in 2018 utilizing the $(Co_{0.2}Cu_{0.2}Mg_{0.2}Ni_{0.2}Zn_{0.2})O$ system [21], demonstrating that entropy-stabilized structures could maintain robust lattice persistence and durable cycling stability. The enhanced electrochemical performance of HEMs is generally attributed to four fundamental core effects: high-entropy effect, severe lattice distortion effect, sluggish diffusion effect, and cocktail effect [18,22,23]. During the past decade, research into high-entropy anodes has expanded exponentially across diverse crystallographic frameworks, including rock-salt [24,25], spinel [26,27], and perovskite [28,29] phases. These materials have demonstrated remarkable performance, often outperforming their low-entropy counterparts.

This review provides a comprehensive summary of the recent

* Corresponding author.
** Corresponding author.
E-mail addresses: ruanwq@szu.edu.cn (W. Ruan), majiang@szu.edu.cn (J. Ma).

https://doi.org/10.1016/j.enrev.2026.100193
Received 2 June 2026; Received in revised form 23 June 2026; Accepted 30 June 2026

progress of the application of HEMs in lithium-based battery anodes. We systematically summarize the roles of HEMs as both active materials and interphase mediators, structured across distinct classifications including HEAs, HEOs, and other high-entropy derivatives. We also discuss current lithium storage mechanisms and the remaining practical challenges. Finally, we offer perspectives on the role of high-entropy systems for emerging energy storage technologies.

2. Definition and fundamental theory of high-entropy materials

HEMs represent a new design philosophy departing from the conventional model of a single-element host matrix supplemented by trace dopants. By occupying a shared crystallographic sublattice with several major atomic species in roughly equal proportions, these systems reveal extensive, untapped compositional regions at the center of multi-element phase diagrams [30,31]. High-entropy materials are fundamentally defined based on two primary criteria: configurational entropy and chemical composition [32].

Configurational entropy (ΔS_{conf}) primarily dictates the formal classification of a high-entropy system, which also serves as a thermodynamic metric for atomic disorder within the lattice [31]. Based on the Boltzmann hypothesis, the molar configurational entropy is quantified as:

$$\Delta S_{conf} = -R\sum_{i=1}^{n} x_i \ln x_i$$

where R is the universal gas constant, n is the number of components, and x_i is the mole fraction of the i-th constituent. In an ideal random state, a threshold of 1.5R is generally accepted as the boundary for high-entropy phases, while materials falling between 1.0R and 1.5R are stratified as medium-entropy, and those below 1.0R are considered low-entropy [33]. Statistically, entropy is maximized when components are present in an equimolar ratio ($x_i = 1/n$), simplifying the expression to $\Delta S_{conf} = R\ln n$. While a binary equimolar system yields only 0.69R, a quinary system (n = 5) reaches 1.61R, thereby fulfilling the criteria for a high-entropy configuration [18,34].

Regarding chemical makeup, HEMs are defined as single-phase solid solutions comprising at least five key elements, with each element's atomic concentration generally held between 5% and 35% [33,34]. The multi-component feature differentiates HEMs from standard alloys, which rely on a primary metal matrix that restricts chemical complexity. The formation of a stable, single-phase structure (such as rock-salt, spinel, or perovskite) is often an entropy-driven process. According to the Gibbs free energy relationship ($\Delta G = \Delta H - T\Delta S$), a sufficiently high ΔS is highly instrumental in driving down the total mixing free energy, thereby promoting system stabilization [35,36]. Entropy-driven stabilization not only broadens the solubility thresholds of otherwise immiscible species but also inhibits the precipitation of brittle intermetallic compounds, thereby ensuring the structural robustness of the materials.

3. The four core effects of high-entropy materials

The anomalous functional and structural properties of HEMs frequently surpass those of their low-entropy counterparts, an optimization universally attributed to the four fundamental core effects [18,22,23,37]. These effects govern the materials' behavior from thermodynamic, structural, kinetic, and functional perspectives.

3.1. High-entropy effect (thermodynamics)

Theoretically, a system's configurational entropy rises sharply when numbers of main elemental species inhabit the same crystallographic sublattice. The resulting high ΔS_{conf} serves as a primary thermodynamic driver to stabilize the system. Under the Gibbs free energy relation ($\Delta G_{mix} = \Delta H_{mix} - T\Delta S_{mix}$), the $T\Delta S$ term grows large enough to offset positive mixing enthalpies, thereby preventing phase separation (Fig. 1a). In the context of electrochemical energy storage, thermodynamic robustness remains critical for expanding solubility limits and facilitating disordered atomic distributions to preserve the crystalline framework [23,38]. Consequently, HEO anodes can maintain their lattice framework even under the repetitive mechanical stress of lithiation/delithiation cycling, significantly extending the cycle life [38,39].

3.2. Severe lattice distortion (structure)

Unlike traditional materials with regular periodic frameworks, HEMs exhibit geometric and chemical heterogeneity due to the random occupancy of ions with disparate radii and varying electronegativities [35,40]. Mismatching atomic radii in the system induces pronounced local displacements and establishes heterogeneous internal strain fields, which fundamentally alter the material's mechanical and transport characteristics (Fig. 1b) [22,38]. Despite increasing electron and phonon scattering (and thus reducing conductivities), these lattice distortions significantly benefit battery performance [41]. The distorted lattice also facilitates the formation of oxygen vacancies and surface defects, which construct low-energy percolation networks that lower ion migration barriers and provide additional active sites for reactions [23,42].

3.3. Sluggish diffusion (kinetics)

Atomic migration slows significantly in HEMs, a kinetic hallmark known as sluggish diffusion. This stems from the disordered distribution of principal species, which creates a complex potential energy landscape [36]. Lattice potential fluctuations then function as atomic traps (Fig. 1c), substantially elevating the activation energy required for substitutional diffusion or vacancy-mediated hopping [23,31]. In battery environments, this kinetic retardation is vital for suppressing harmful phase transitions, grain coarsening, and active material pulverization, thereby ensuring the mechanical persistence of the electrode framework over extended cycling [40].

3.4. Cocktail effect (properties)

Synergistic interactions among constituent species—the cocktail effect—yield collective properties that exceed a simple weighted average of individual components. The cocktail effect provides a paradigm for strategically balancing components with disparate functions (Fig. 1d). In HEO anodes, for instance, electrochemically inactive spectator elements (e.g., Mg or Al) structurally stabilize the host crystalline framework, whereas multivalent transition metal cations (e.g., Co, Ni, and Fe) serve as active redox centers to deliver faradaic storage capacity [43–46]. Ultimately, the cocktail effect enables HEMs to circumvent the rigid stoichiometric constraints of traditional materials, offering a versatile platform for optimizing charge transfer kinetics and overall electrochemical functionality.

4. Application of high-entropy materials in lithium-based anodes

While the four core effects provide a robust theoretical framework for the stability and unique properties of high-entropy systems, their practical significance is best realized through their integration into specific electrochemical environments. In the context of lithium-based anodes, the thermodynamic, structural, and kinetic advantages afforded by high entropy serve as the physical foundation for overcoming the intrinsic limitations of traditional electrode materials. By synergistically modulating ion migration barriers, accommodating mechanical strain, and providing versatile redox centers, these fundamental effects directly govern the performance of high-entropy materials across the three

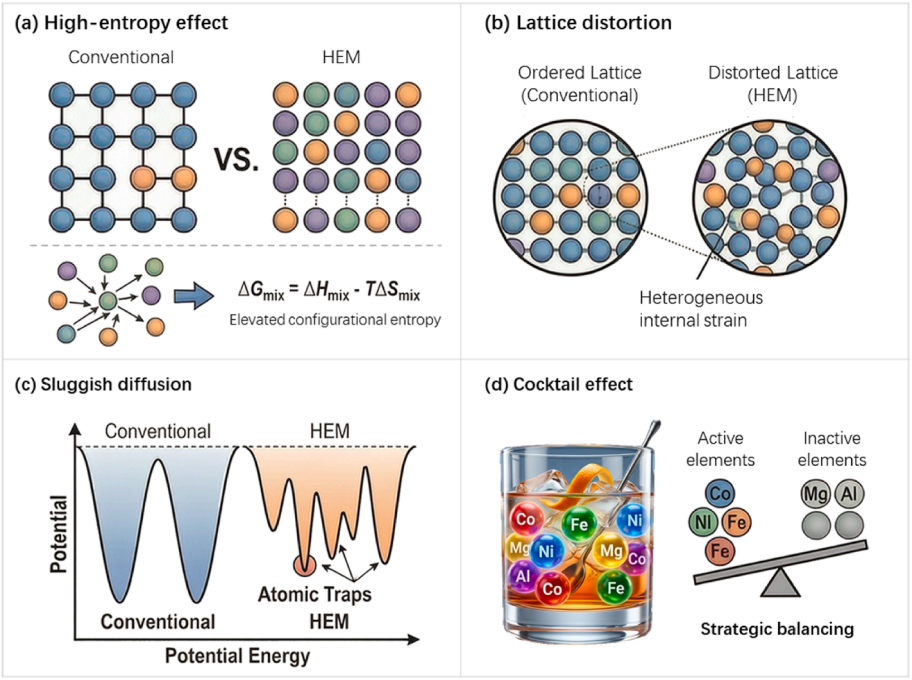

Fig. 1. The four fundamental "core effects" of HEMs: (a) High-entropy effect, (b) Lattice distortion, (c) Sluggish diffusion, (d) Cocktail effect.

primary storage pathways: intercalation, alloying, and conversion (Table 1).

Intercalation anodes like graphite and $Li_4Ti_5O_{12}$ have host lattices that reversibly insert Li^+ via intercalation with minimal volume change [6,47]. Conversely, alloying anodes like silicon form alloys with lithium and offer massive capacity but suffer from 300% volume expansion [48]. Conversion anodes, meanwhile, rely on redox reactions with transition compounds (e.g., Fe_2O_3 [49], Co_3O_4 [50]) to yield nanoscale particles within a Li_2O matrix [51]. Despite their high capacities, conversion anodes are impeded by large voltage hysteresis, low initial Coulombic efficiency (CE), and profound structural reconstruction [52,53]. Because these mechanisms are fundamentally governed by the active elements present, HEM anodes inevitably fall into these three categories or operate through a combination of these pathways. In the following sections, we will detail how the unique attributes of high-entropy materials are translated into superior electrochemical performance within diverse compounds.

4.1. *High-entropy alloys*

High-entropy alloys, typically composed of at least five metallic elements, offer a versatile platform for battery anodes due to their tunable electrochemical properties, which are governed by both their constituent elements and chemical states. These HEAs can be broadly categorized into two types: with and without active elements. In this part, we will summarize the application of high-entropy alloys in lithium-based battery anodes.

4.1.1. *High-entropy alloy without active elements*

When comprised of zero-valent elements immune to further reduction or lithiation-induced alloying, the HEA framework acts primarily as an interfacial mediator rather than a direct capacity contributor. In this role, HEAs leverage the cocktail effect to provide abundant lithiophilic sites that regulate lithium metal deposition. A primary application of this kind of HEAs lies in the surface engineering of anodes, such as a 20-nm conformal NiCdCuInZn HEA coating (conceptually designated as "tights") engineered by Wang et al. [54] on carbon fibers, as shown in Fig. 2a and b. By utilizing gradient absorption energies (−3.18 to −2.03 eV) provided by the variety of elements, this configuration lowers the barrier for Li nucleation. Operando monitoring of the lithium-ion flux verified that the HEA nanoparticles accelerate local Li migration (Fig. 2c) and ensure a uniform initial nucleation for subsequent deposition. Such an HEA/C anode achieves a lifespan of 7200 h (at 60 mA cm^{-2}/60 mAh cm^{-2}) in symmetric cells and 160 cycles at 1C with an average CE of 99.5% in an anode-free NCM811 pouch cell. Subsequent work with CuInNiSnCd [57] nanoparticles grown on carbon fiber demonstrated that full substrate coverage might not be a prerequisite for performance gains, as partial HEA decoration also significantly enhances cycle performance of the carbon fiber anode. Regarding high-rate performance, AlMnCoNiFe nanoparticles on carbon cloth (HEA-NPs-CC) [55] have been demonstrated to preserve their structural morphology during fast charging, with in-situ TEM (Transmission Electron Microscopy) characterization revealing negligible volume expansion (Fig. 2d and f). The formation of Li-Al alloys within this framework effectively lowers nucleation barriers and accelerates kinetics. Consequently, HEA-NPs-CC||NCM811 full cells with a lean N/P ratio of 1 exhibited 85.76% capacity retention at 1C after 260 cycles, as shown in Fig. 2e.

In lithium-metal batteries, the anode exhibits high reactivity toward electrolytes. Parasitic reactions between the deposited lithium metal and the electrolyte lead to the irreversible consumption of the lithium source and electrolyte depletion during cycling, resulting in low CE and limited cycle life. To mitigate these degradation pathways, artificial solid electrolyte interphases (SEIs) are extensively deployed to alleviate side reactions, with lithium fluoride (LiF) being a critical component. Recently, research has focused on the synergistic effects of HEA modification and artificial SEIs to further enhance the performance of lithium anodes.

Drawing inspiration from the high-entropy concept, Liu et al. [58] proposed an in-situ modification protocol to construct a hybrid

Table 1
Storage mechanism of lithium ions in three kinds of anodes.

Reaction type	Anode materials	Reaction formula
intercalation	Graphite (Gr.)	$6C + xLi^+ + xe^- \rightleftharpoons Li_xC_6$ (x is normally 1)
Alloying	Silicon(Si)	$Si + xLi^+ + xe^- \rightleftharpoons Li_xSi$ ($0 \leq x \leq 4.4$)
conversion	Fe_2O_3	$Fe_2O_3 + 6Li^+ + 6e^- \rightleftharpoons 2Fe + 3Li_2O$

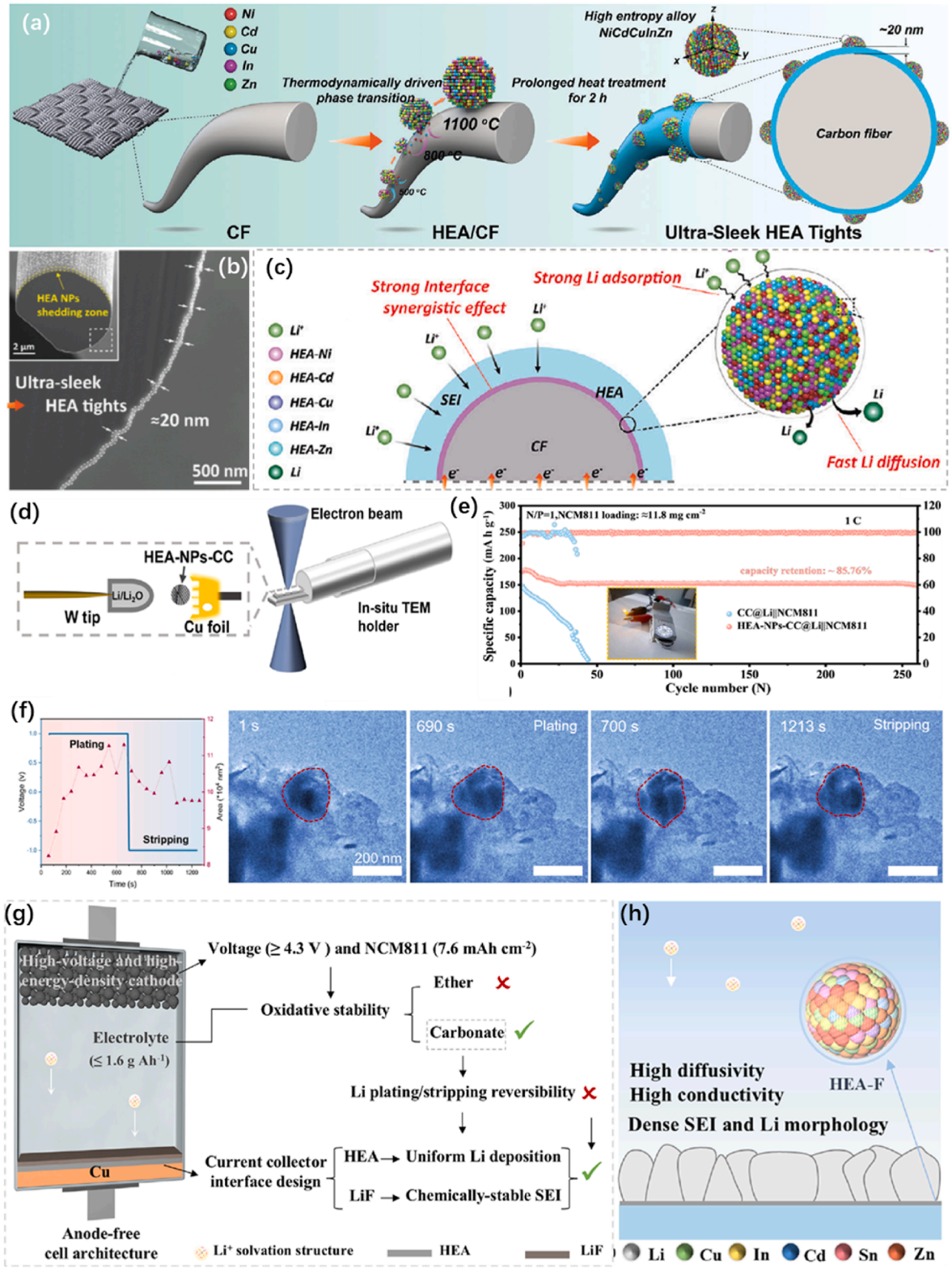

Fig. 2. (a) Schematic illustration of the fabrication of the ultrasleek HEA tights. (b) The FE-SEM of HEA/C. (c) Schematic illustration of Li adsorption and migration over the HEA/C anode. Reproduced with permission from Ref. [54], Copyright 2023, Wiley-VCH GmbH. (d) A schematic illustration of in-situ TEM observation of the electrochemical reaction. (e) The cycling performance of full cells at 1 C. (f) Time-lapse TEM images of the Li plating/stripping process on HEA-NPs at ±1 V: the change of applied electric field and projection area of selected particle as a function of time. Reproduced with permission from Ref. [55], Copyright 2025, Elsevier B. V. (g) Design strategies of the Cu-HEA-F substrate. (h) Schematic illustration of the Li plating on the Cu-HEA-F substrate. Reproduced with permission from Ref. [56], Copyright 2025, Elsevier B.V.

interphase enriched with a multi-element alloy (Sb-Sn-Ag-Al, SSAA) and LiF. A porous, lithiophilic scaffold is directly formed on the Li metal surface through a spontaneous chemical reaction. In this hybrid architecture, the SSAA components provide abundant nucleation sites to ensure uniform Li deposition, while the LiF layer effectively shields the anode from electrolyte-driven degradation. This robust, low-impedance interface enables thin Li||NCM811 pouch cells to retain 70% of their capacity over 400 cycles. In a parallel approach, Hu et al. [56] engineered a dual-layered interphase (Cu-HEA-F) on copper current collectors for anode-free batteries, which integrates an inner CuInCdSnZn HEA layer to maximize lithiophilicity with an outer LiF layer to stabilize the SEI (Fig. 2g). The Cu-HEA-F induced a significantly denser Li deposition compared to that on a pristine Cu current collector, as illustrated in Fig. 2h. By mitigating the rapid lithium depletion inherent in anode-free systems, this strategy allowed 2.5 Ah pouch cells to achieve a high energy density of 380 Wh kg^{-1} under stringent

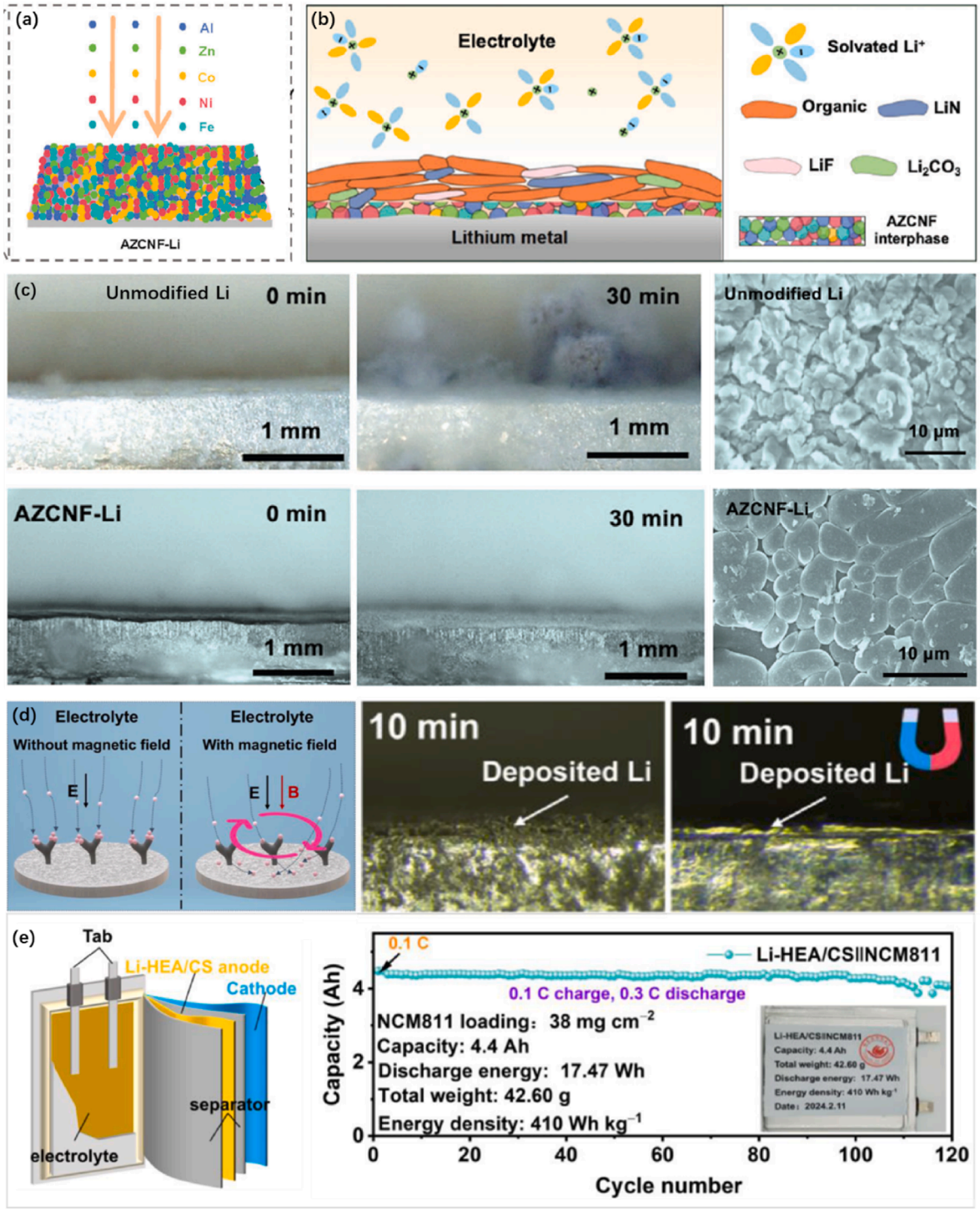

Fig. 3. (a) Schematic diagram of AZCNF HEA interphase and (b) the lithium plating on it. (c) In situ optical microscopy of Li^+ deposition on unmodified Li and AZCNF-Li, and their corresponding SEM images. Reproduced with permission from Ref. [59], Copyright 2024, Wiley-VCH GmbH. (d) Li^+ trajectory and deposition with and without a magnetic field. (e) Structure and cycling performance of Li-HEA/CS||NCM811 pouch cells. Reproduced with permission from Ref. [60], Copyright 2025, Elsevier B.V.

lean-electrolyte and high-loading conditions.

Beyond chemical modification, recent innovations have introduced multi-physical field regulation. Zheng et al. [59] constructed an amorphous Al-Zn-Co-Ni-Fe (AZCNF) interphase that uses a horizontal Lorentz force to redirect lithium-ion flux, ensuring uniform lithium metal deposition (Fig. 3a–c). The unprecedented mechanical strength and anti-corrosion properties of this modified layer further stabilize the anode interface, yielding robust cycling stability exceeding 4000 h at 2 mA cm^{-2}. Jin et al. [60] extended this magneto-electrochemical synergy to PtCuFeCoNi-encapsulated carbon spheres. In this electromagnetic-coupled field, the flux trajectory of Li ions follows a spiral motion toward the anode base, as shown in Fig. 3d, promoting a dense and uniform deposition of lithium. The corresponding Li-HEA/CS||LFP full cells obtain 90.1% capacity retention after 800 cycles at 1C, and a high-energy-density stacking Li-HEA/CS||NCM811 pouch cell achieved a practical energy density of 410 Wh kg^{-1} (Fig. 3e).

To bypass labor-intensive trial-and-error, machine learning (ML) is used to screen HEA compositions. Researchers deployed advanced algorithms, such as XGBoost and Random Forest, to identify optimal configurations (e.g., Al-Zn-Fe-Co-Ni) by evaluating critical descriptors including mechanical hardness, lithiophilicity, and electronic conductivity. Using SHAP analysis, scientists have quantified the roles of component elements, discovering that while aluminum ensures structural strength due to the local mismatch of its radius, zinc is what truly enhances Li binding energy. Beyond composition, ML-driven strategies like particle swarm optimization (PSO) were successfully employed to refine experimental parameters, such as magnetron sputtering power and time, based on predicted CE of Li||Cu half cells. These integrated computational-experimental approaches yielded dense, amorphous interphases that effectively suppress dendritic propagation and global volume variations, achieving prolonged stability for over 2400 h and high-rate performance up to 10 mA cm^{-2} [61].

The application of HEAs without active elements has transitioned from passive nucleation coatings to versatile interphases that regulate ion flux through both chemical cocktail effects and physical field interactions. These sophisticated designs have successfully addressed dendrite growth inherent in lithium metal and anode-free systems. The successful integration of these alloys into high-energy-density pouch cells marks a significant step toward commercial viability. Machine learning-guided high-throughput screening will be essential to further explore the vast compositional landscape of HEAs, potentially uncovering robust materials with resilient SEI interphase and augmented low-temperature performance.

4.1.2. *High-entropy alloy with active elements*

Integrating active elements such as Si, Ge, and P into HEAs enables them to undergo reduction and alloying reactions with lithium, delivering significant effective capacity. In contrast to traditional alloying and conversion materials that often suffer from severe volume changes and sluggish kinetics [62,63], HEAs with active components ease these issues through configurational stabilization.

Silicon-based anodes are a primary focus for high-energy-density lithium-ion batteries, notwithstanding their severe volume expansion. Su et al. [64] synergized high-entropy and amorphization strategies for thin-film (TF) anodes, utilizing an all-lithium-reactive system (Si, Al, Mg, Ge, Sn, and Zn) to facilitate a solid-solution reaction mechanism (Fig. 4a). This structural paradigm successfully eliminates the severe, stress-concentrating phase boundaries characteristic of pristine Si, thereby mitigating electrode pulverization (Fig. 4b and c). The stable amorphous matrix—composed of Si, Al, Mg, and Ge—effectively buffers volume changes, while segregated Sn nanocrystals within the matrix accelerate Li^+ transport kinetics. Consequently, the optimized $Si_{50}(AlMgGeSn)_{12.5}$ (5-HEATF) anode demonstrated remarkable durability with 94.6% capacity retention after 50 cycles, a stark contrast to the 14.3% retention of pure Si thin films after only 20 cycles.

Extending from composition to structure, Ding et al. [65] engineered a multilevel nanoporous SiGeTiZnCuAl medium-entropy alloy (NP-MEA) with a 3D metallic sponge architecture as shown in Fig. 4d. The architecture featuring interconnected pore channels serves as a mechanical buffer that cushions the strain from volume expansion during lithiation. Simultaneously, the intentional mismatch in atomic radii and electronegativity promotes electron redistribution across the electrode, thereby significantly boosting charge-transport kinetics. Addressing the needs for commercial scalability, Park et al. [66] integrated high-entropy silicon alloys (HESiA, Fig. 4e) into the graphite anode, and the specific capacity of the composite anode elevates with increasing silicon content (Fig. 4f). They synergized the stability of HESiA with high-conductivity carbon networks, achieving a 92–95% capacity retention over 100 cycles and a high rate capability at 7C with this anode.

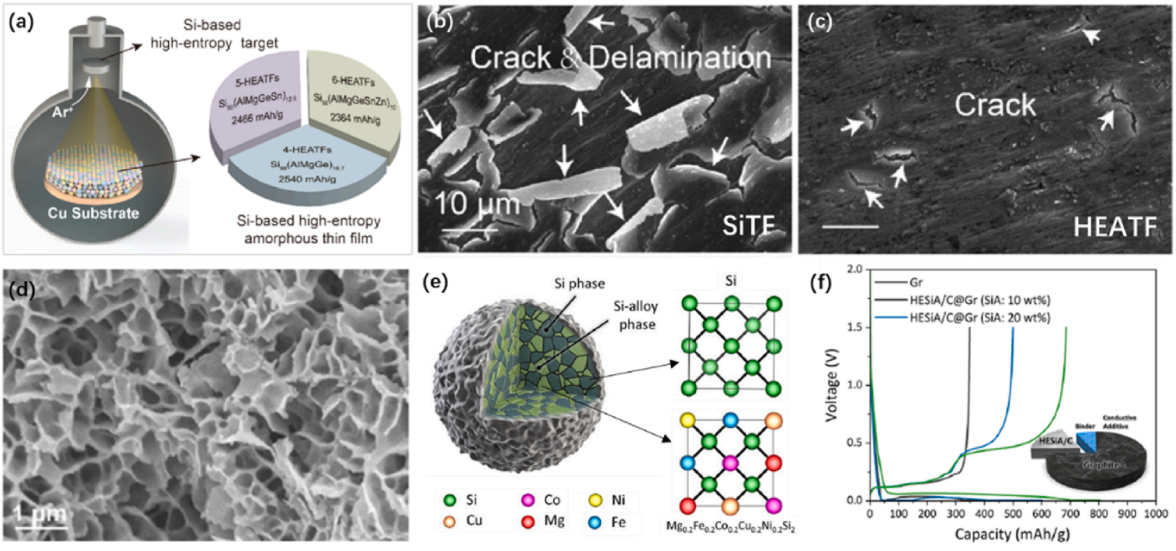

Fig. 4. (a) Schematic diagram of the preparation of HEATFs. SEM images comparison of (b) SiTF and (c) HEATF after cycling. Reproduced with permission from Ref. [64], Copyright 2024, Elsevier B.V. (d) SEM image of NP-MEA. Reproduced with permission from Ref. [65], Copyright 2024, Elsevier B.V. (e) Schematic representation of HESiA particle and crystal structures of Si and metal silicide. (f) Charge/discharge curve of Gr and HESiA/C@Gr. Reproduced with permission from Ref. [66], Copyright 2026, Springer Nature.

In addition to Si, high-entropy strategies are also proven effective for improving the performance of chalcogen- and pnictogen-based systems. Zhao et al. [67] developed a SnSbMnBiTe (HE-SSMBT) HEA that effectively circumvents the massive volume fluctuations inherent in alloying-type anodes. This design achieved a non-visible volume expansion (≈1.9%) during lithiation, enabling a high volumetric capacity of 2408.4 mAh cm^{-3} at 0.1 A g^{-1}. Multi-element synergy drives this record-low strain by facilitating self-adaptive relaxation. Notably, the HE-SSMBT also exhibits remarkable low-temperature performance, delivering 1418 mAh cm^{-3} even at −30 °C, thus paving the way for all-climate battery applications.

HEA engineering provides a powerful approach to stabilize the alloying and conversion types of anodes. Coupled with hierarchical architecture design, their performance can be further improved toward their theoretical limits while ensuring unmatched durability and fast-charging capability. The future trajectory for HEA anodes lies in the convergence of data-driven composition screening and hierarchical structure design.

4.2. High-entropy oxides

Building upon the structural stabilization strategies developed for HEAs, HEOs represent a distinct but related class of materials characterized by metal cations in positive valence states, despite their similar high-entropy properties. When an HEO material is used as an anode, the multivalent constituent metallic cations undergo electrochemical reduction, thereby contributing substantial faradaic capacity in the initial charge of the batteries. Regarding these electrochemical characteristics, HEOs exhibit intrinsic similarities to conventional TMOs, as both frameworks host multivalent transition-metal cations that drive the primary redox reactions. According to previous research, TMO anodes suffer from severe volume expansion, particle pulverization, and surface passivation during the lithiation/delithiation cycling, which impedes their practical application [68,69]. HEO anodes outperform TMO anodes with better lattice resilience, representing a robust evolution of conventional TMO systems [35]. In this section, we will briefly summarize recent advances in the application of HEOs in the anodes of lithium-based batteries.

4.2.1. Composition and structure engineering of HEOs

Since the first single-phase HEO ($Mg_{0.2}Co_{0.2}Ni_{0.2}Cu_{0.2}Zn_{0.2}$)O [70] with a rock salt (Fig. 5a) structure was synthesized in 2015, various new structures, including spinel (Fig. 5c), perovskite, and fluorite, have emerged. The primary challenge in designing a target HEO phase lies in selecting constituent metal cations that satisfy crystallographic constraints while balancing entropy-driven stabilization with thermodynamic stability. According to the extended Hume-Rothery rules for solid solution formation, the final structure depends on properties of constituent elements, including atomic size difference, electronegativity, valence electron concentration, and crystal structure compatibility [35]. According to the extended Hume-Rothery rules, solid-solution stabilization requires satisfying the following three empirical criteria:

(1) Atomic radius difference (Δδ): $\Delta\delta \leq 6\%$
(2) Electronegativity difference (Δχ): $\Delta\chi \leq 0.2$
(3) Average cation valence (n): $+2.0 \leq n \leq +2.5$

A recent study, involving single-element extraction from the $(CrMnFeCoNiZn)_3O_4$ system to generate a series of five-metal HEOs, has demonstrated that high-valence cations such as Cr, Mn, and Fe are essential for maintaining a pure cubic spinel phase [72]. In a typical AB_2O_4 spinel structure, higher-valence cations (mostly trivalent) are required to occupy the B-sites. The removal of Cr, Mn, or Fe leads to an excess of divalent cations relative to the available trivalent sites, which induces the formation of a secondary rock-salt phase, although the spinel phase remains dominant in such compounds. Their results also demonstrate the distinct roles of each element during the electrochemical process: Fe serves as the primary capacity contributor, Ni and Zn function as performance stabilizers, and Co exhibits minimal impact on structural or electrochemical behavior. This differentiation highlights the critical role of elemental selection in compositional engineering.

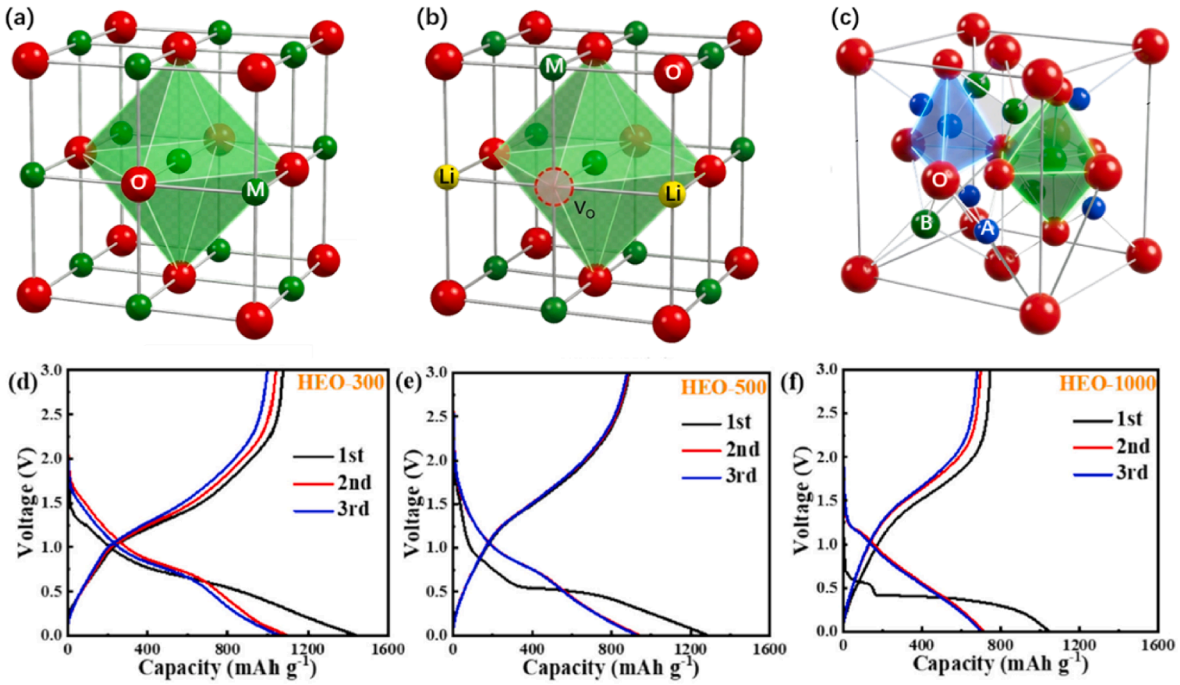

Fig. 5. (a) Rock salt structure (MO). (b) Rock salt structure (MO) with Li^+ substitutions and oxygen vacancies. (c) Spinel structure AB_2O_4. (d-f) Discharge/charge curves for initial 3 cycles for HEO-300/500/1000. Reproduced with permission from Ref. [71], Copyright 2025, Elsevier B.V.

Another study has investigated cobalt-free $(FeNiCrMnMgAl)_3O_4$ [45], which maintains a spinel structure, consistent with prior findings about the role of Co, and achieves competitive electrochemical performance. In this system, the Mg and Al species, forming in-situ MgO and Al_2O_3, act as electrochemically inactive "spectators" to construct a robust mechanical buffering matrix, whereas transition metals such as Fe, Ni, Cr, and Mn serve as active redox centers. The buffering matrix effectively mitigates volume fluctuations and prevents nanoparticle agglomeration during the conversion reactions. Such a spectator effect enables a unique, reversible, stress-induced spinel-to-rock salt phase transition and preserves a short-range ordered crystal structure even in the fully lithiated state—a sharp contrast to most spinel HEOs, which typically undergo amorphization upon full lithiation [73].

Other high-valence cations, such as Ti^{4+} and V^{5+}, are also incorporated into HEOs. Studies confirm that Ti maintains a stable valence state throughout electrochemical cycling, acting as a redox-inactive structural anchor or matrix, similar to the spectator role of Mg. This prevents the aggregation of active transition metals and the breakdown of the structural framework [74]. In contrast, vanadium is characterized by a highly flexible, multivalent nature (ranging from V^{5+} to V^{2+} or even V^0), which facilitates multi-electron transfer and significantly boosts the specific faradaic capacity. During deep lithiation, high-valence V^{5+} can be reduced to lower oxidation states or metallic vanadium (V^0). This process contributes to charge storage while simultaneously improving electronic conductivity and increasing oxygen vacancy concentrations. Structurally, Vanadium also enhances rigidity through strong V–O bonding, which effectively buffers mechanical stress and curbs volume expansion to just ~6.64% after 100 cycles [75].

To be used as anodes in batteries, the materials should also have ion diffusion paths for the transport of Li^+. For example, ion migration from 8a to 16c is the main pathway in the spinel structure, while migration happens in the rock salt structure through cation vacancies [35,76]. Defect engineering is one of the common strategies to accelerate ion diffusion. For HEO materials, the increase of oxygen vacancies was found to promote the Li^+ diffusion and electronic conductivity [42]. Substituting the high valence cations with low valence ones like lithium is an effective approach to introduce oxygen vacancies into the compounds, as shown in Fig. 5b. Mozdzierz et al. [77] proved that $(Co\text{-}Cu\text{-}Mg\text{-}Ni\text{-}Zn)_{1-x}Li_xO$ exhibits unique mixed ionic-electronic conduction due to the presence of oxygen vacancies. The battery performance based on the $[Li_x(Cr_{0.2}Fe_{0.2}Ni_{0.2}Mn_{0.2}Cu_{0.2})_{1-x}]_3O_4$ ($x = 0$, 0.05, 0.1) anode is better than that based on its undoped counterpart HEO anode [78]. Similar results are also found in other lithium-doping HEO, accompanied by a higher capacity [46,76,79]. Podgornova et al. [80] compared the multi-anionic and multi-cationic $Li_{0.5}(Co_{0.2}Cu_{0.2}Mg_{0.2}Ni_{0.2}Zn_{0.2})_{1.5}O_{1.5}F_{0.5}$ ($x = 0.5$) with the original $(Co_{0.2}Cu_{0.2}Mg_{0.2}Ni_{0.2}Zn_{0.2})O$ and demonstrated that the former one performs better due to a higher Li^+ diffusion conductivity. However, the role of fluoride ions has not been discussed, and its necessity remains unknown. Chen et al. [25] introduced lattice distortion into the rock salt HEO $(Mg_{0.2}Co_{0.2}Ni_{0.2}Cu_{0.2}Zn_{0.2})O$ by low-temperature post-annealing. The concentration of crystal defects, which increases with prolonged annealing time, actually has a reverse trend to the oxygen vacancy concentration. The HEO with the most serious lattice distortion has the best performance due to the enhanced electronic conductivity, indicating that lattice distortion plays a more important role than oxygen vacancy in this material.

The influence of crystallinity has also been investigated by systematically tuning heat treatment temperatures from 300 to 1000 °C. Wang et al. [71] demonstrated that increasing the annealing temperature causes the material to evolve from an amorphous state (HEO-300) to a highly crystalline spinel structure (HEO-1000) without phase segregation. These structural differences lead to distinct electrochemical behaviors (Fig. 5d–f): HEO-1000 displays a flat discharge plateau, and the amorphous HEO-300 conversely exhibits a large initial discharge slope, indicating a successive intercalation/deintercalation process. According to the results, a starting amorphous structure appears to be favored, as HEO-300 achieved a better cycling performance than HEO-1000. High defect concentrations and lower volume expansion rates in the amorphous matrix are the main contributors, as they provide additional active sites and suppress particle pulverization during long-term cycling, respectively.

The electrochemical performance of various HEO-based anodes is summarized in Table 2 for ease of review and comparison. To ensure clarity, only the compositions yielding the optimum cycling performance are shown for a series of closely related HEOs in the same paper. Missing capacity retention data in the original literature are denoted by "/". Most investigated HEO anodes adopt a spinel structure. The relative scarcity of rock-salt and perovskite types suggests a more limited compositional diversity in these structural families than in the spinel phase. Therefore, we will mainly focus on spinel-type HEOs in this section.

4.2.2. Morphology control of HEOs

Despite the benefits of entropy-driven stabilization, HEOs often face practical hurdles such as sluggish kinetics and volume expansion. To address these challenges, morphology control has emerged as an effective approach for developing high-performance anodes in lithium-ion batteries [35,97]. Researchers have dedicated themselves to developing HEOs with unique features, such as yolk-shell structures [83,98] and multishelled designs [99]. Zhao et al. [100] compared three different morphologies, including nanoparticles, nanosheets (Fig. 6a), and core-shell spheres (Fig. 6b), and demonstrated that core-shell structures exhibit optimized performance. With a robust mechanical shell, this structure serves as a buffer layer to mitigate internal stress and accommodate the significant volume expansion typically associated with conversion-type reactions. The porous feature of this structure provides a high specific surface area for electrochemical reactions, and the structural resilience also effectively prevents particle pulverization and aggregation.

Similarly, the novel duplex yolk–shell structure (DYSHEO, Fig. 6c) [98] extends these benefits by connecting two yolk-shell particles into a peanut-like architecture. Sharing common advantages with core-shell designs, the large connected hollow interiors of DYSHEO provide significant free volume to mitigate structural strains and buffer the mechanical stress induced by repeated lithium-ion insertion. This cavity-rich morphology increases the electrode-electrolyte contact area and shortens diffusion pathways, ensuring rapid reaction kinetics. In addition to these volumetric benefits, the integration of an isogenic amorphous/crystalline heterophase within this structure offers distinct advantages; while the crystalline regions provide conductivity and mechanical support, the amorphous regions offer an open-frame structure that further accommodates volume expansion and provides additional lithium storage sites. The resulting built-in electric field at the heterophase interfaces enhances ion adsorption and diffusion, leading to a reversible capacity of approximately 1721 mAh g^{-1} and robust cycling stability.

Building upon these architectural designs, Xu et al. [101] explored the morphological transition of $(FeCoNiMnCrMg)_2O_3$ from solid spheres to multishelled core–shell spheres (C-HEO, Fig. 6d) and hollow spheres (H-HEO), governed by thermally induced shrinkage and the Kirkendall effect. Both C-HEO and H-HEO provide large surface areas, but the finite element simulations show that the hollow H-HEO is preferred for managing mechanical strain. Specifically, C-HEO structures suffer from stress superposition due to the lithiation rate difference between the inner core and outer shell, whereas the hollow design allows for a more uniform distribution of stress, conferring augmented structural durability and reversible capacity.

A more complicated shell-and-cavity design is achieved in hollow multishelled structures HEO $(LiFeZnNiCoMn)_3O_4$ (HoMS-HEO) as shown in Fig. 6e [99]. Ordered shells and internal voids grant this 3D architecture multi-level buffering advantages. The multiple shells act as

Table 2
The performance of lithium-ion batteries based on HEO anodes.

Structure	Composition	Battery type	Cycling performance: Specific capacity (mAh g^{-1}) (cycles)	current density (mA g^{-1})	capacity retention	Year	Reference
Spinel	$(FeCoNiCrMn)_3O_4$	HEO||Li	402 (300)	500	/	2020	[81]
Spinel	$(FeCoNiCrMn)_3O_4$	HEO||Li	596.5 (1200)	2000	86.2%	2022	[82]
Spinel	$(NiMnCrCoFe)_3O_4$	HEO||Li	526.8[a] (300)	5000	99.8%	2023	[44]
Spinel	$(FeCoNiCrMn)_3O_4$	HEO||Li	679.3 (300)	500	/	2025	[71]
Spinel	$(CrFeMnNiCo)_3O_4$	HEO||Li	~900 (250)	500	94%	2025	[83]
Spinel	$(FeCoCrNiMn)_3O_4$	HEO||Li	579.5 (3000)	1000	/	2025	[84]
Spinel	$(FeCoCrNiMn)_3O_4$	HEO||$LiFePO_4$	100.4 (100)	500	97.3%	2025	[84]
Spinel	$((FeCoNiCrMnXLi)_3O_4$ (X = Cu, Mg, Zn): $(FeCoNiCrMnZnLi)_3O_4$	HEO||Li	522.1 (100)	500	/	2021	[76]
Spinel	$(FeNiCrMnMgAl)_3O_4$	HEO||Li	670 (1200)	200	99.8%	2021	[73]
Spinel	$(FeNiCrMnMgAl)_3O_4$	HEO||Li	458.75 (1000)	1000	90.5%	2025	[45]
Spinel	$(CrMnFeNiCu)_3O_4$	HEO||Li	747 (250)	1500	99%	2022	[27]
Spinel	$(FeCrNiMnZn)_3O_4$	HEO||Li	642.8 (200)	500	~100%	2025	[85]
Spinel	$(CrMnFeCoCu)_3O_4$	HEO||Li	275 (312)	500	80%	2024	[86]
Spinel	$(CoNiZnXMnLi)_3O_4$ (X = Fe, Cr): $(CoNiZnFeMnLi)_3O_4$	HEO||Li	605 (100)	100	84%	2022	[87]
Spinel	$(CoNiZnXMnLi)_3O_4$ (X = Fe, Cr): $(CoNiZnFeMnLi)_3O_4$	HEO||$LiCoO_2$	260.2 (100)	500	76.6%	2022	[87]
Spinel	$(CrMnFeCoNiZn)_3O_4$-(X): $(MnFeCoNiZn)_3O_4$	HEO||Li	667.3 (350)	500		2025	[72]
Spinel	$(Zn_{0.2}Mn_{0.2}Fe_{0.2}Co_{0.2}Ni_{0.2})_3O_4$	HEO||Li	757.8 (1000)	1000	/	2025	[88]
Spinel	composite from the oxidation of HEA AlCrFeCoNi	HEO||Li	543 (1000)	500	/	2023	[89]
Spinel	$(FeCoMgCrLi)_3O_4$	HEO||Li	658 (200)	200	/	2024	[79]
Spinel	$(FeCoMgCrLiZn)_3O_4$	HEO||Li	800 (300)	200	/	2025	[90]
Spinel	$(Fe_{0.2}Co_{0.2}Ni_{0.2}Cr_{0.2}Zn_{0.2})_3O_4$	HEO||Li	203 (1000)	3000	/	2025	[91]
Spinel	$(CoMnZnNiMg)_2CrO_4$	HEO||Li	608 (200)	200	94.8% (compared to 3rd cycle)	2023	[92]
Spinel	$(Cr_{0.2}Mn_{0.2}Co_{0.2}Ni_{0.2}Zn_{0.2})_3O_4$	HEO||Li	107 (1000)	1000	/	2024	[93]
Spinel	$(VCrNiCoMn)_3O_4$	HEO||Li	733 (1000)	200	72%	2025	[75]
Spinel	$(XTiZnNiFe)_3O_4$ (X = Co, Mg)	HEO||Li	Co: 130 (800) Mg: 100 (800)	1000	Co: 43%[a] Mg: ~100%	2023	[74]
Spinel	porous hollow $(NiCoCuFeMg)_3O_4$	HEO||Li	907 (300)	2000	~100%	2024	[94]
Spinel	$(Al_{0.2}Mn_{0.2}Co_{0.2}Ni_{0.2}Zn_{0.2})_3O_4$	HEO||Li	350 (1000)	1000	/	2026	[95]
Rock slat	$Mg_{0.2}Co_{0.2}Ni_{0.2}Cu_{0.2}Zn_{0.2}O$	HEO||Li	920 (300)	100	/	2019	[96]
Rock slat	(LiMgCoNiCuZn)O	HEO||Li	417 (300)	1000	83%	2022	[42]
Rock slat	$Mg_{0.2}Co_{0.2}Ni_{0.2}Cu_{0.2}Zn_{0.2}O$	HEO||Li	365 (300)	2000	/	2022	[24]
Rock slat	$(Co_{0.2}Cu_{0.2}Mg_{0.2}Ni_{0.2}Zn_{0.2})O$	HEO||Li	771 (400)	1000	/	2024	[25]
Perovskite	$[(Bi,Na)_{0.2}(La,Li)_{0.2}(Ce,K)_{0.2}Ca_{0.2}Sr_{0.2}]TiO_3$	HEO||Li	120.4 (300)	1000	~100%	2020	[29]
Perovskite	$La(Co_{0.2}Mn_{0.2}Fe_{0.2}Ni_{0.2}Cu_{0.2})O_3$	HEO||Li	Not provided	/	/	2025	[28]

[a] Calculated data.

inter-supporting units that accommodate volume expansion while simultaneously shortening the effective diffusion distance for both ions and electrons. In situ characterizations verify that HoMS-HEO maintains unwavering architectural form, exhibiting a negligible volume change of only about 3% even after long-term cycling.

Taking a distinct approach to the hollow framework, Gao et al. [102] utilize hollow graphene microspheres as a conductive skeleton for the in situ deposition of rock-salt-type HEO nanoparticles (RHEO@TrGO) (Fig. 6f). This design retains the cavity effect, where the hollow interior acts as an electrolyte reservoir to minimize ion transport resistance. However, it transcends standard hollow HEO shells in two fundamental aspects. First, the conductive graphene shell establishes a far more efficient electron diffusion network compared to pure oxide shells, which often suffer from sluggish kinetics. Furthermore, the defect-enriched graphene framework serves as a robust template; its unique surface chemistry suppresses the severe particle aggregation and agglomeration typically observed in pure HEOs during high-temperature calcination. This synergy between the carbonaceous hollow framework and high-entropy nanoparticles facilitates accelerated reaction kinetics and a significant capacity-increase phenomenon, achieving nearly 1400 mAh g^{-1} after 800 cycles.

Morphology engineering has become a quintessential technique for overcoming the inherent kinetic and mechanical hurdles of HEO anodes. Designing architectures with efficient diffusion pathways, such as hollow shells, has proven effective in mitigating volume expansion while simultaneously accelerating ion transport. A deeper exploration of the synergistic effects between tailored composition, phase control, and morphology construction is required to further optimize performance. Mastering these structural and compositional interplays will be essential for translating the high-capacity potential of HEOs into practical, long-life commercial battery technologies.

4.2.3. Lithium storage mechanisms of high-entropy oxide anodes

The diverse compositional, structural, and morphological strategies discussed in the preceding section establish a versatile foundation for HEO anode optimization. Furthermore, elucidating the lithium storage mechanisms of these materials is essential for tailoring their properties to meet the requirements of specific battery applications. To understand the fundamental impact of the high-entropy effect, density functional theory (DFT) calculations are employed to reveal that the high-entropy configuration underpins the dramatic improvement in electrochemical performance by synergistically optimizing electronic structure and lattice robustness. For instance, in the $(Fe_{0.2}Co_{0.2}Ni_{0.2}Cr_{0.2}Zn_{0.2})_3O_4$ (FCNCZO) model HEO, the high-entropy configuration induces strong metal-oxygen orbital hybridization and broadens the d-band width, effectively eliminating the electronic bandgap to facilitate rapid electron transport. Similarly, the $(FeCoNiCrMn)_3O_4$ HEO exhibits a drastically narrowed bandgap of 0.084 eV, which is significantly lower than the 3.407 eV bandgap found in traditional Co_3O_4 [82].

Beyond electronic enhancements, the random distribution of

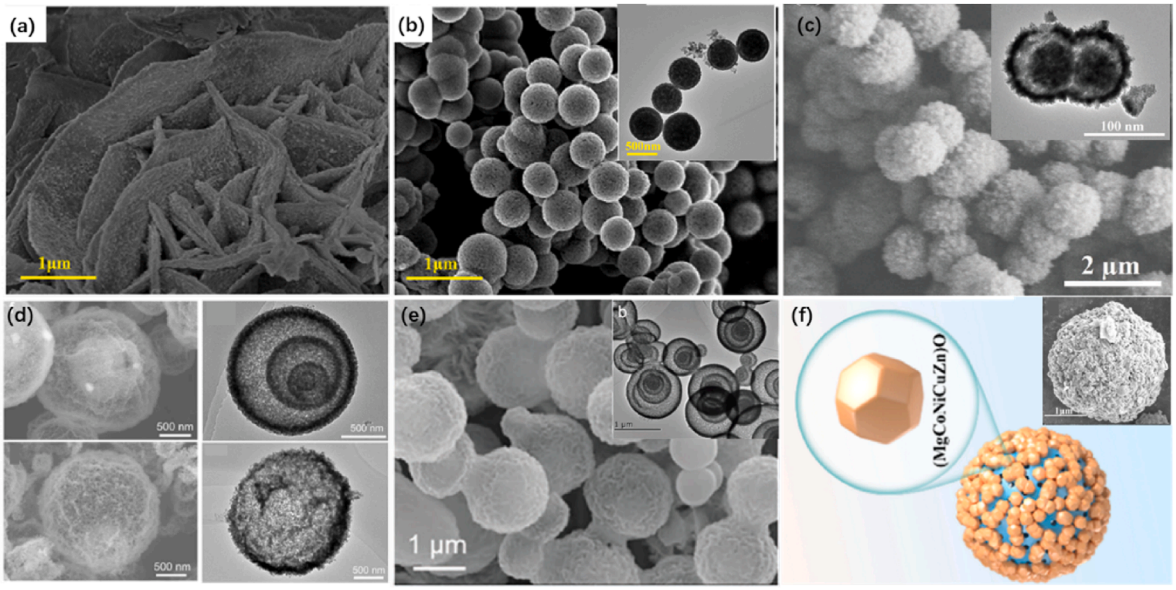

Fig. 6. SEM images and corresponding TEM images of HEO with different morphology: (a) nanosheet, (b) core-shell sphere, Reproduced with permission from Ref. [100], Copyright 2025, Elsevier B.V. (c) duplex yolk–shell, Reproduced with permission from Ref. [98], Copyright 2024, Wiley-VCH GmbH. (d) multishelled core–shell spheres (C-HEO) and hollow spheres (H-HEO), Reproduced with permission from Ref. [101], Copyright 2025, Springer Nature. (e) hollow multishelled. Reproduced with permission from Ref. [99], Copyright 2024, Wiley-VCH GmbH. (f) Schematic diagram and SEM image of RHEO@TrGO. Reproduced with permission from Ref. [102], Copyright 2025, American Chemical Society.

multiple metal cations leads to significant lattice distortion and a high concentration of oxygen vacancies. These features effectively shorten lithium-ion diffusion pathways and increase the density of active redox sites. Such a configuration promotes internal charge redistribution, enabling a multi-element synergistic redox mechanism and a high pseudocapacitive contribution that ensures a high-rate capability. Crucially, the entropy stabilization effect mitigates the mechanical stress associated with conversion reactions, thereby suppressing nanoparticle fracture and preserving the electrode's structural cohesion during prolonged cycling [91].

Detailed investigations into the lithiation/delithiation processes in spinel-structured HEOs have revealed complex, sometimes divergent structural pathways. Wang et al. [81] identified a unique amorphization reaction process in $(FeCoNiCrMn)_3O_4$, where the long-range ordered spinel lattice, upon discharge to 0.01 V, undergoes structural rearrangement into a stable amorphous state that maintains uniform elemental distribution during subsequent cycles without detectable segregation (Fig. 7a). Conversely, using the same material, Jin et al. [84] observed a pathway where the spinel structure evolves into a rock salt structure in the initial discharge and only partially recovered to form a mixed spinel/rock-salt hybrid and ultimately stabilizes as a pure rock-salt phase after cycling (Fig. 7b). The structural evolution into a rock-salt phase involves the synergistic migration of multivalent cations from tetrahedral to octahedral sites. This process is thermodynamically

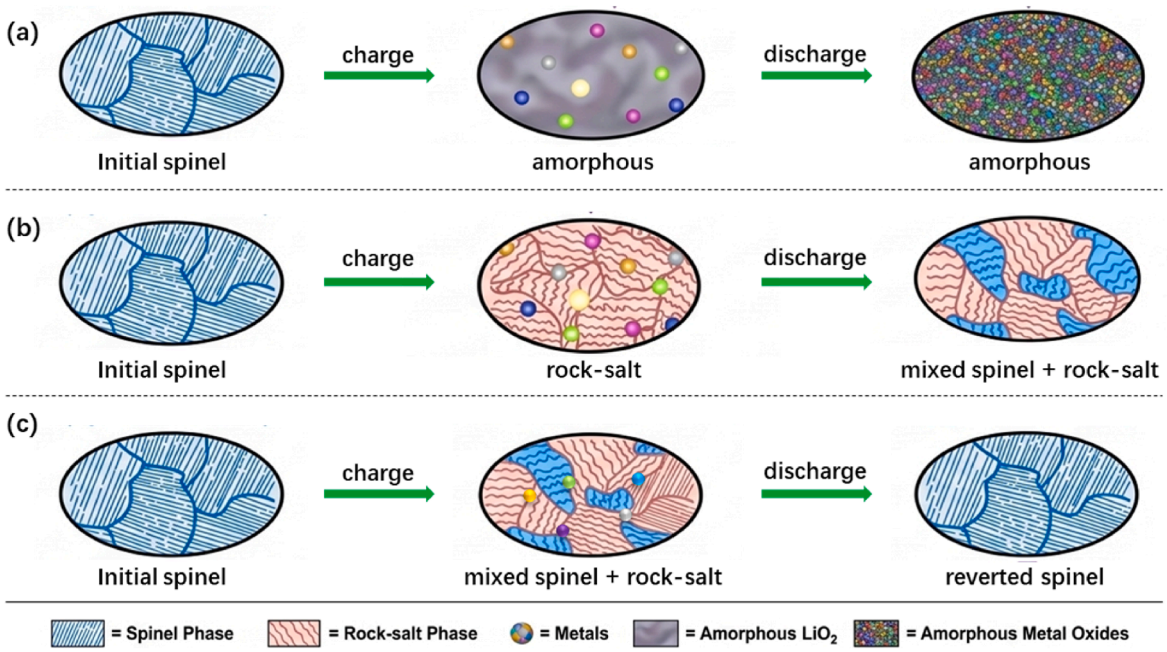

Fig. 7. Schematic illustration of different structural evolutions of HEO anodes during the lithiation/delithiation process.

driven by the lower formation energy of the rock-salt phase (−2.08 eV) compared to the spinel phase (−1.96 eV). This energetic preference, coupled with kinetic limitations during delithiation, ensures the persistence of the rock-salt framework.

This prominent scientific divergence regarding the final lithiated state of an identical chemical composition highlights a major debate in the field and underscores the critical influence of synthetic parameters. The fundamental differences in the synthesis protocols and resulting morphologies likely govern these distinct phase transition routes. Wang et al. synthesized the HEO via a conventional high-temperature solid-state reaction of mixed oxides, yielding relatively large, smooth sub-micron particles (200 - 900 nm). The larger particle size and associated sluggish diffusion kinetics restrict long-range atomic reorganization during lithiation, forcing the lattice to collapse into a disordered, amorphous state to accommodate volume-expansion-induced stress. In contrast, Jin et al. employed an innovative arc-melting and dealloying process followed by calcination, producing highly uniform, fine nanoscale octahedra with an average size of ~126 nm. The substantially reduced dimensions and unique defect chemistry inherited from the dealloying method impart greater lattice flexibility and shorten atomic diffusion distances. This structural advantage enables the constituent atoms to overcome kinetic barriers and reorganize into a thermodynamically stable crystalline rock-salt phase, rather than undergoing complete amorphization. Therefore, the initial particle size, morphology, and synthetic lineage appear to critically dictate the phase transition pathways in HEO anodes. To firmly establish this paradigm, however, further in-depth investigations into the underlying atomistic mechanisms remain essential.

A similar spinel-to-rock-salt phase transition was also observed in a cobalt-free HEO $(FeNiCrMnMgAl)_3O_4$ by Guo et al. and Zheng et al., suggesting that such a transition may be a common phenomenon for spinel HEOs [45,73]. Specifically, Zheng et al. utilized in-situ XRD (X-ray Diffraction) to demonstrate that this phase transformation is reversible, with the structure being repaired back to a better crystalline spinel after charging (Fig. 7c). Their work also uniquely identified a spinel phase residue phenomenon, where a portion of the parent spinel phase is maintained throughout the cycling process. By inducing the same phase transformation through high-energy ball milling, they concluded that the transition is a stress-induced, diffusion-free continuous phase transition [73]. These studies reveal that transition metal cations (Fe, Ni, Cr, and Mn) undergo partial conversion reactions rather than full reduction, allowing the entropy-stabilized framework to function as a stable host matrix. This resilience is further attributed to the spectator effect of inactive components like MgO and Al_2O_3, which effectively buffer volume changes and stabilize the crystalline structure [45].

A more granular picture of these dynamics is provided by Triolo et al. through ex-situ synchrotron XAS (X-ray absorption spectroscopy) analysis of $(MnFeCoNiZn)_3O_4$ nanofibers. This study detailed an irreversible multi-step lithiation process involving lithium insertion, cation migration, and an incomplete conversion reaction. In detail, Fe, Co, and Ni cations reduce to their metallic states in the order Fe < Co < Ni, whereas Mn undergoes partial reduction (Mn^{4+} to Mn^{3+}/Mn^{2+}) and does not fully revert to its pristine state upon re-oxidation. Therefore, there should be some residual metal oxides (including Li_2O) or metals inside the anode after the initial discharge/charge cycle. A distinctive feature is the behavior of Zn^{2+} cations, which do not participate in the conversion reaction but instead migrate from tetrahedral (8a) to octahedral (16d/16c) sites. This migration, facilitated by a high concentration of oxygen vacancies (40.6%), triggers the phase transition and opens lattice channels for rapid Li^+ transport [26].

In contrast, rock-salt structured HEOs like $(Mg_{0.2}Co_{0.2}Ni_{0.2}Cu_{0.2}Zn_{0.2})O$ exhibit a different mechanism where the crystalline framework holds for approximately 60% of capacity before collapsing into an amorphous state. The cations follow a sequential reduction in the order of Cu-Co-Ni under lithiation in the voltage range between 1.2V and 0.7V, which entails irreversible conversion, metallic/oxide coexistence, and significant cation segregation, showing poor configuration stability compared to spinel HEOs. Notably, this rock-salt HEO also features a unique alloying-dealloying mechanism involving the reduction of Zn and Mg to form Li-Zn and Li-Mg alloys, which contribute significantly to reversible charge storage [103].

Notwithstanding the consensus on the importance of the high-entropy effect for structural resilience, significant divergences exist regarding whether the structural evolution is reversible during lithiation/delithiation and whether the final lithiated state of spinel HEOs is a stable amorphous framework or a reorganized rock-salt lattice. These discrepancies are not only related to compositions and crystalline structures but also likely arise from other unknown impacts, such as morphology, highlighting the structural flexibility of high-entropy systems. Determining which secondary phase—amorphous or crystalline—provides optimal long-term stability and better performance will be essential for the rational design of anode materials. Future research should also investigate whether the observed cation segregation in rock-salt HEOs is a universal limitation or a challenge that can be overcome through precise elemental tuning.

4.2.4. *Practical issues of high-entropy oxide anodes*

Despite the reported performance superiority of HEO anodes over traditional TMOs, several critical operational hurdles have received insufficient attention. During lithiation/delithiation cycles, HEO crystalline structures undergo a complex evolution dictated by their initial compositions, crystalline structures, and other unclear influences. Throughout this process, HEOs can transition through various states, including pure crystalline, mixed crystalline, and partially or fully amorphous phases. Because their electrochemical behavior is state-dependent—and these states themselves are a product of the electrochemical history—the structural evolution of HEOs is inherently complicated and unpredictable. Consequently, poor consistency may lead to significant cell-to-cell variations, potentially causing catastrophic failures in large-scale battery modules.

Another practical challenge is the distinct capacity rebound exhibited by HEO anodes, characterized by a sharp initial capacity drop followed by a gradual recovery over extended cycling, as shown in Fig. 8a [82,88,101,104]. The initial decay in the cycling is primarily attributed to the dynamic formation and restructuring of the SEI layer and the irreversible generation of Li_2O during the conversion process. The high specific surface area of HEO nanoparticles promotes the continuous growth of thick, unstable SEI layers that consume active lithium ions and can physically encapsulate active materials, leading to electrochemical deactivation. The subsequent capacity recovery and stabilization, typically beginning after dozens of cycles, is driven by the structural activation of the electrode and the maturation of the SEI. Repeated lithiation/delithiation cycles induce volume changes that expose previously isolated active sites and generate nanoscale pores or defects, thereby creating new and shorter pathways for ion transport. Mechanistically, this enhancement is often associated with pseudocapacitive interface storage (Fig. 8b and c), where a polymeric/gel-like layer is reversibly formed and dissolved on the surface of the active material, augmenting the storage capacity [51,91,95,105].

Such a subsequent capacity rise may appear to extend cycle life, but it poses significant challenges for battery management systems (BMS). These systems rely on linear and predictable capacity models to accurately estimate state of charge (SOC) and state of health (SOH). Therefore, these non-linear, fluctuating capacity profiles can trigger unacceptable estimation errors [106,107]. Additionally, because the capacity recovery is typically induced by pseudocapacitive behavior, it often induces significant voltage hysteresis and reduces overall round-trip energy efficiency. In large-scale battery packs, this non-linear behavior exacerbates cell-to-cell inconsistency, as varying activation rates among individual cells can trigger premature pack failure and serious safety concerns [108]. Establishing a standardized method to

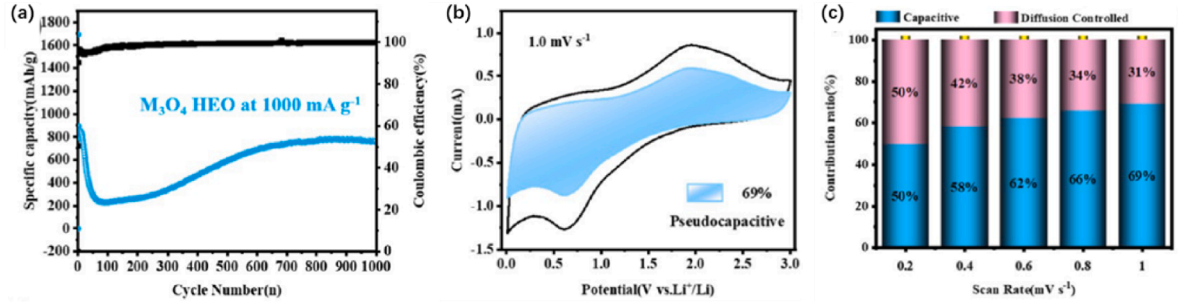

Fig. 8. (a) Long-term cycling performance of M_3O_4 HEO anode showing an initial capacity decay with a following capacity increase. (b-c) Pseudocapacitive contribution under different scan rates. Reproduced with permission from Ref. [88], Copyright 2025, American Chemical Society.

scientifically assess cycling stability under such circumstances remains an unresolved challenge.

From a practical and engineering standpoint, the severe capacity drop in the initial cycles inevitably correlates with a very low initial CE and a massive irreversible consumption of active lithium. In commercial full-cell configurations (such as the HEO||$LiFePO_4$ system), this continuous active lithium depletion is a fatal drawback that severely restricts the overall energy density and cycle life. To effectively regulate the active lithium inventory and mitigate the severe early-stage lithium consumption inherent to HEO anodes, pre-lithiation has emerged as a compelling industrial strategy. By integrating supplementary active lithium into either the cathode or the anode before cell assembly, this approach successfully counterbalances initial capacity losses, thereby boosting the ICE, cycling lifespan, and practical energy density of full cells [109]. Nevertheless, executing these techniques introduces distinct technical challenges. For instance, uncontrolled or excessive lithium incorporation can distort the host HEO crystal lattice, trigger detrimental phase separation, and ultimately compromise the structural integrity of the electrode, which directly undermines the structural stabilization intended by the high-entropy design. Furthermore, a stringent trade-off persists between energy density and cycle life. While optimized pre-lithiation prolongs cycling stability, the introduction of bulky carrier reagents or the accumulation of electrochemically inactive byproducts increases the dead weight of the electrode, thereby penalizing the overall specific energy [110,111]. Consequently, precisely calibrating the pre-lithiation dosage to perfectly synchronize with the complex, non-linear capacity evolution of HEOs stands as a pivotal frontier for their commercial realization.

4.3. Other high-entropy materials

4.3.1. High-entropy sulfides and selenides (HESs/HESes)

High-entropy sulfides and selenides (HESs/HESes) are witnessing a surge in research interest within the battery community due to their versatile component adjustability, lattice endurance, and better electrical conductivity compared to traditional binary transition metal sulfides (TMSs) [112,113]. Although traditional TMSs possess rich redox chemistry, they are prone to large volume change during cycling, leading to SEI breakage and electrode pulverization [112,114]. High-entropy design addresses these issues through entropy stabilization and lattice distortion, which can suppress particle aggregation and crack propagation [113]. Alvi et al. [115] stabilize such complex conversion-alloying reactions via the formation of a medium-entropy $BiSbSe_{1.5}Te_{1.5}$ (BSST). This material achieves outstanding cycling stability without the need for carbonaceous composites, which are conventionally required to prevent pulverization in simple metal chalcogenide anodes. The BSST anode delivers a staggering volumetric capacity of 3224 mAh cm^{-3}, nearly five times that of commercial graphite, while retaining its high-entropy structural characteristics throughout cycling.

Due to their compositional similarities, HESs/HESes typically exhibit parallel electrochemical behaviors to HEOs. Consequently, performance-optimization strategies employed for HEO anodes are highly applicable to HES/HESe systems. As a prime example, innovative nanoarchitectures have been engineered to further boost HES performance. Specifically, yolk–shell structured (CrMnFeCoNi)S_2 and (CrMnFeCoNi)Se_2 nanospheres [112] provide abundant void space to cushion volume expansion and shorten ion/electron diffusion pathways. Furthermore, the weak short-range order inherent in these materials creates additional diffusion channels, thereby accelerating reaction kinetics. Driven by the synergistic "cocktail effect" of multiple metal ions on the increased storage capacity, the (CrMnFeCoNi)S_2 electrode demonstrated a high specific capacity of 1375.8 mAh g^{-1} after 1250 cycles at 1 A g^{-1}.

Advanced synthesis and interface engineering have also broadened the application of HESs. Carbon encapsulation, such as in (FeCoNiCuZn)S_x/C nanocomposites [114] derived from ZIF-8, significantly strengthens the composite architecture and electron transfer. Furthermore, high-pressure and high-temperature (HPHT) synthesis has been utilized to create pressure-stabilized (FeCoNiCuRu)S_2 [113], overcoming energy barriers to alloy otherwise immiscible elements like ruthenium. This pressure-stabilized HES showed excellent long-term stability with over 85% capacity retention after 15,000 cycles at 10 A g^{-1}. Additionally, nanostructured HES (e.g., WMoNbZrVS_x) [116] in-situ formed on carbon fiber through sulfurization was employed as a lithiophilic interface in anode-free lithium metal batteries, where its multi-site surface facilitates non-selective lithium deposition and promotes dense, uniform lithium growth (Fig. 9a). The anode-free HES/CF||$LiFePO_4$ full cell showed a low capacity decay rate of 0.053% at 0.5C rate within 700 cycles, which is much better than the undecorated CF anode as shown in Fig. 9b.

4.3.2. High-entropy anodes with multiple Li-active elements: silicon and phosphide systems

In contrast to TMOs and TMSs, high-capacity anode materials — such as Si, P, and Sn —display distinct electrochemical signatures, as they undergo unique alloying or conversion reactions to deliver high specific capacities during lithiation. However, large volume expansion and mechanical pulverization during lithiation obstruct the industrial adoption of these anode materials, leading to low initial CE and rapid capacity degradation of the batteries. To address these challenges, the emerging high-entropy design strategy integrates multiple Li-active elements into single-phase or atomically disordered systems to alter the electrochemical response from concentrated stress to a harmonious, multi-step lithiation process.

High-entropy silicon-based materials exhibit immense promise for mitigating the intrinsic brittleness of silicon during lithiation by transitioning it to a ductile state. A primary innovation in this field is the development of micron-sized Si-based HEAs, such as the CrMnFeCoNiSiGe [117] system. As shown in Fig. 9d, the reversible capacities of these anodes are closely related to the molar ratio of Si and Ge, as all of them are active to Li. In these HEAs, the diffusion retardation effect prevents

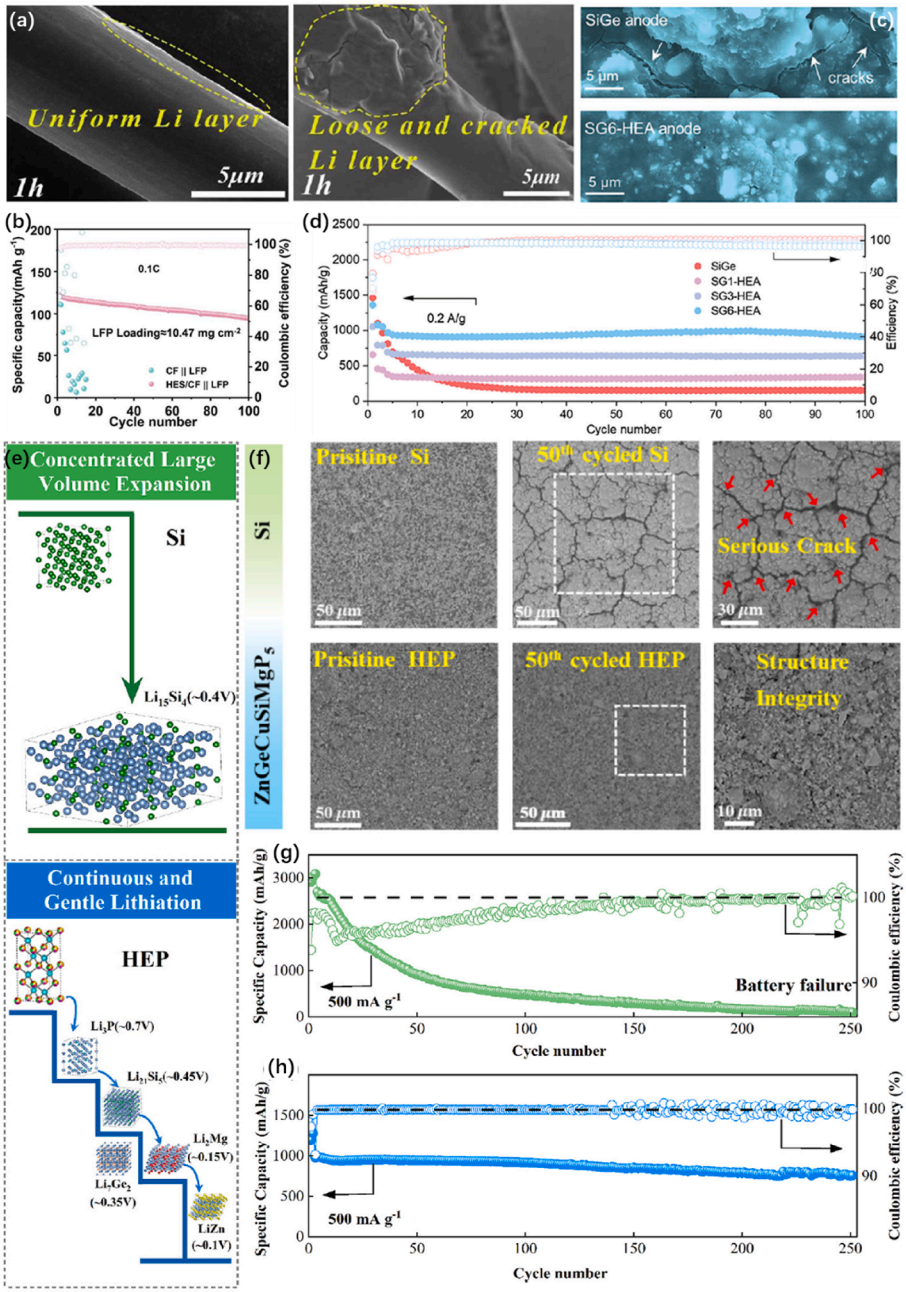

Fig. 9. (a) Comparison of lithium deposition morphology on HES/CF and pristine CF. (b) Cycling performance of LFP batteries with different anodes. Reproduced with permission from Ref. [116], Copyright 2026, Springer Nature. (c) SEM images of SiGe and SG6-HEA anodes after 20 cycles. (d) Cycling performance of batteries with SiGe and SiGe-based HEM anodes. Reproduced with permission from Ref. [117], Copyright 2023, Wiley-VCH GmbH. (e) The comparison of Li storage mechanisms of Si and HEP anodes. (f) SEM images of Si and HEP anodes before and after 50 cycles. (g,h) Cycling performance of Si/C and HEP anodes at 500 mA g^{-1}. Reproduced with permission from Ref. [118], Copyright 2026, Elsevier B.V.

chemical phase separation of transition metals during lithium insertion, allowing transition metal elements to remain uniformly doped within the Li_x(Si/Ge) lattice as substituted atoms. Theoretical simulations reveal that this doping strengthens metallic bonding and reduces anisotropic stress, therefore increasing the ductility of the lithiated HEAs and enabling fewer cracks in the anodes after cycling, as shown in Fig. 9c.

The integration of high-entropy chemistry with sophisticated nano-architectures, such as the hierarchical 3D honeycomb-inspired Si@HE@C composites [119], involves embedding Si nanoparticles and high-entropy phases within a continuous 3D honeycomb carbon framework. The honeycomb channels provide buffering space for Si expansion while the high-entropy metallic elements catalyze the graphitization of the carbon scaffold, enhancing both electrical conductivity and mechanical robustness. These composites maintain a reversible capacity of 1203.53 mAh g^{-1} after 100 cycles.

In addition to Si, metal phosphide is another type of anode material that offers a high theoretical capacity for advanced LIB anodes. Theoretically, the incorporation of nonmetallic element P into the HEA usually induces the formation of high-entropy phosphide (HEP). Similar to the O element in HEOs, the nonmetallic element P usually occupies a specific anionic position in the crystal and contributes no capacity during the lithiation process. Consequently, the reaction mechanisms of these materials depend heavily on the constituent metal cations, mirroring the behavior of HEOs. For example, the NiCoFeMnCrP [120] nanoparticles with 3d transition metal cations probably undergo a multi-step reduction of the cations during the lithiation process. The transition metals are found to boost electronic conductivity and facilitate lithium-ion diffusion, which ensures an excellent cyclic stability and rate capability of the anode. Research indicates that the selection of metal precursors, such as nitrates over chlorides, can notably enhance capacity retention, with nitrate-derived NiCoFeMnCrP achieving 409 mAh g^{-1} after 230 cycles.

Expanding the scope to Si-included phosphide, a multi-cationic

phosphide $ZnGeCuSiMgP_5$ [118], which crystallizes in a sphalerite cubic structure, was also investigated. The uniqueness of this HEP is the incorporation of alloying elements, including Ge and Si. This HEP enables a continuous and gentle multi-electron lithiation process (e.g., sequentially forming Li_3P, Li_xSi/Ge, and Li_xZn/Mg) across a wide potential range (0.7 V to 0.1 V), effectively avoiding the concentrated large volume expansion and serious cracks typical of single-element anodes like silicon (Fig. 9e and f). Both Ge and Si can exhibit an alloying reaction after the conversion reaction and therefore promote the capacity. Such structural optimization also results in faster charge transfer and significantly higher lithium diffusivity compared to commercial Si/C anodes. Consequently, $ZnGeCuSiMgP_5$ electrodes deliver a reversible capacity of 758 mAh g^{-1} at 0.5A g^{-1} after 250 cycles (Fig. 9g and h) and an unrivaled rate performance (436.5 mAh g^{-1} at 5 A g^{-1}).

There are also some amorphous or atomic-disordered high-entropy compounds with P fabricated and used as anodes. Wei et al. [121] designed and fabricated an atomic-disordered Ge-Sn-Sb-Si-Fe-Cu-P HEA. By strategically selecting Li-reactive elements (Ge, Sn, Sb, Si, P) for capacity and high-conductivity elements (Fe, Cu) for electron transport, this HEA shows a large discharge capacity of 1448 mAh g^{-1}. Although the author categorized this material as an HEA, the metal-P bond connection indicates that it is likely a HEP. To further address the volume expansion issues, the HEA nanoparticles (3–5 nm) are encapsulated in a carbon matrix via high-energy ball milling to form a dragon-fruit-like HEA/C composite. The electrical connection and interphase cohesion of the anode are promoted through the formation of P-C or P-O-C chemical bonds between the HEA and the carbon matrix. As a result, the HEA/C composite restricts volume expansion to 25%–34% (compared to >300% for pure elements) and maintains long-term cycle stability (>1600 h). Another cost-effective alternative, the amorphous Sn-Si-Co-Cu-P HEA/graphite composite [122] without Ge has been developed. This system utilizes a graphite wrapping strategy to establish a conductive network, maintaining 1196.5 mAh g^{-1} after 1000 cycles.

In contrast to HEOs and HESs, which primarily utilize transition metal cations as active species, HEPs derive their massive capacities from non-transition metal or metalloid elements such as Si, Ge, and Sn. This compositional distinction fundamentally alters their electrochemical behavior: HEO and HES anodes typically mimic the conversion-type mechanisms of conventional TMOs, whereas HEP anodes are dominated by alloying-type processes. Despite these differences, both categories exhibit improved performance compared to their traditional counterparts, a benefit directly attributable to the structural stabilization afforded by the high-entropy strategy. To propel this field forward, integrating machine learning and AI for targeted composition design will be crucial to reconcile the trade-off between ultrahigh capacity and long-term structural endurance. Ultimately, establishing cost-effective and scalable synthesis protocols remains the vital bottleneck to transition these advanced materials from academic half-cells to practical, high-performance full-battery applications.

5. Summary and outlook

The emergence of HEMs represents a paradigm shift in the design of high-performance anodes for lithium-based batteries. By moving beyond traditional single-element systems, HEMs—including high-entropy alloys (HEAs), oxides (HEOs), sulfides (HESs), and phosphides (HEPs)—leverage the synergy of the four core effects (high entropy, lattice distortion, sluggish diffusion, and the cocktail effect) to achieve performance levels unattainable by conventional materials. In the context of anodes, high-entropy strategies have proven effective in stabilizing conversion and alloying structures, thereby mitigating the severe volume expansion and rapid capacity decay that plague traditional TMOs and silicon-based materials [123,124]. Despite the rapid expansion of research into various high-entropy compounds, the field remains in its infancy and faces several critical hurdles.

To transition these materials from laboratory innovation to industrial application, the following research directions are proposed:

1. Accelerated material discovery via artificial intelligence and machine learning: The astronomical compositional space inherent to HEMs renders traditional empirical trial-and-error methodologies prohibitively inefficient and resource-intensive. Future research must prioritize the integration of ML and AI to predict phase stability, screen for chemical compatibility, and optimize related physicochemical descriptors. By synergizing these computational tools with automated high-throughput synthesis, researchers can evaluate vast candidate compositions, rapidly identifying those with favorable electrochemical properties, like enhanced ionic conductivity and suitable redox potentials.
2. Mechanism elucidation: Despite significant progress in materials optimization, the precise lithium storage mechanisms in high-entropy systems remain contentious. Specifically, the factors governing crystalline structural evolution and the optimal phase configuration for anode applications have yet to be fully clarified. To bridge this gap, advanced in situ and operando characterization techniques are indispensable for tracking atomic-scale structural transitions, valence state fluctuations, and the specific role of oxygen vacancies during cycling. These efforts are essential to provide foundational insights for the rational design of high-entropy anodes.
3. Overcoming practical electrochemical Bottlenecks: High-entropy anodes currently suffer from a low initial CE and a high content of conductive carbon additives, which significantly reduce the overall energy density. Furthermore, the non-linear capacity evolution (initial decay followed by a gradual rise) typical of HEOs poses significant challenges for BMS. Targeted strategies, such as surface coating and nanostructural engineering, must be refined to address these issues.
4. Transitioning from lab-scale to practical systems: The prevailing half-cells with small electrodes in publications provide only fundamental insights. The practical realization of HEM anodes, however, hinges on full-cell performance with larger capacity. Future efforts must shift toward evaluating HEM anodes within full-cell environments, with a particular focus on their compatibility with advanced electrolytes, high-voltage cathodes, and functional binders. As the battery landscape evolves toward all-solid-state architectures, uncovering the electrochemical behavior of HEMs in solid-state systems will be paramount to bridging the gap between fundamental discovery and industrial application.

In conclusion, while significant scientific and engineering obstacles remain, the unique lattice-level strength and tunability of HEMs offer a revolutionary platform to resolve the inherent conflicts between high capacity and cycling stability in battery anodes. Through interdisciplinary collaboration across materials science, data science, and electrochemistry, HEMs are poised to drive transformative advances in the global energy storage landscape.

Declaration of competing interest

The authors declare that they have no known competing financial interests or personal relationships that could have appeared to influence the work reported in this paper.

Acknowledgements

This work was financially supported by the Key Area Research and Development Program of Guangdong Province (Grant No. 2024B0101070001), the NSF of China (Grant Nos. 52401217, 52571191, 52271150, 52571190), the Advanced Materials-National Science and Technology Major Project (Grant No. 2025ZD0619204), the Natural Science Foundation of Guangdong Province (Grant No. 2026A1515010279), the Science, Technology and Innovation

Commission of Shenzhen Municipality (Grants No. RCJC20221008092730037, JCYJ20250604182240052, JCYJ20240813141413018), the Research Team Cultivation Program of Shenzhen University (Grant No. 2023QNT001).

References

[1] M.M. Hasan, R. Haque, M.I. Jahirul, M.G. Rasul, I.M.R. Fattah, N.M.S. Hassan, M. Mofijur, Advancing energy storage: the future trajectory of lithium-ion battery technologies, J. Energy Storage 120 (2025) 116511.

[2] N. Nasajpour-Esfahani, H. Garmestani, M. Bagheritabar, D.J. Jasim, D. Toghraie, S. Dadkhah, H. Firoozeh, Comprehensive review of lithium-ion battery materials and development challenges, Renew. Sustain. Energy Rev. 203 (2024) 114783.

[3] Z.-W. Gao, T. Lan, H. Yin, Y. Liu, Development and commercial application of lithium-ion batteries in electric vehicles: a review, Processes 13 (2025) 756.

[4] X. Liu, Y. Zeng, W. Yuan, G. Zhang, H. Zheng, Z. Chen, Advances in multi-scale design and fabrication processes for thick electrodes in lithium-ion batteries, Energy Rev. 3 (2024) 100066.

[5] K.R. Ngoy, V.T. Lukong, K.O. Yoro, J.B. Makambo, N.C. Chukwuati, C. Ibegbulam, O. Eterigho-Ikelegbe, K. Ukoba, T.-C. Jen, Lithium-ion batteries and the future of sustainable energy: a comprehensive review, Renew. Sustain. Energy Rev. 223 (2025) 115971.

[6] Y. Dong, C. Liu, M. Rui, X. Zhang, Y. Guan, L. Chen, Q. Huang, M. Wang, Y. Su, F. Wu, N. Li, Review on graphite anodes for fast-charging lithium-ion batteries: mechanism, modification and characterizations, Adv. Funct. Mater. 35 (2025) 2506190.

[7] W. Li, X. Sun, Y. Yu, Si-, Ge-, Sn-based anode materials for lithium-ion batteries: from structure design to electrochemical performance, Small Methods 1 (2017) 1600037.

[8] Y. Cui, Silicon anodes, Nat. Energy 6 (2021) 995–996.

[9] G. Wang, M. Aubin, A. Mehta, H. Tian, J. Chang, A. Kushima, Y. Sohn, Y. Yang, Stabilization of Sn anode through structural reconstruction of a Cu–Sn intermetallic coating layer, Adv. Mater. 33 (2021) 2003684.

[10] H. Ying, W.-Q. Han, Metallic Sn-based anode materials: application in high-performance lithium-ion and sodium-ion batteries, Adv. Sci. 4 (2017) 1700298.

[11] X. Xiao, X. Li, S. Zheng, J. Shao, H. Xue, H. Pang, Nanostructured germanium anode materials for advanced rechargeable batteries, Adv. Mater. Interfac. 3 (2016) 1600798.

[12] C. Zhao, S. Yao, C. Li, Y. An, S. Zhao, X. Sun, K. Wang, X. Zhang, Y. Ma, Recent advances in transition metal oxides as anode materials for high-performance lithium-ion capacitors, Chem. Eng. J. 497 (2024) 154535.

[13] J. Du, Q. Li, J. Chai, L. Jiang, Q. Zhang, N. Han, W. Zhang, B. Tang, Review of metal oxides as anode materials for lithium-ion batteries, Dalton Trans. 51 (2022) 9584–9590.

[14] G.F. Ishraque Toki, M. Khalid Hossain, W. Ur Rehman, R.Z. Abbas Manj, L. Wang, J. Yang, Recent progress and challenges in silicon-based anode materials for lithium-ion batteries, Ind. Chem. Mater. 2 (2024) 226–269.

[15] J. Zhu, Y. Ding, Z. Ma, W. Tang, X. Chen, Y. Lu, Recent progress on nanostructured transition metal oxides as anode materials for lithium-ion batteries, J. Electron. Mater. 51 (2022) 3391–3417.

[16] H. Xu, H. Li, X. Wang, The anode materials for lithium-ion and sodium-ion batteries based on conversion reactions: a review, Chemelectrochem 10 (2023) e202201151.

[17] J.W. Sturman, E.A. Baranova, Y. Abu-Lebdeh, Review: high-entropy materials for lithium-ion battery electrodes, Front. Energy Res. 10 (2022) 862551.

[18] T.G. Ritter, S. Pappu, R. Shahbazian-Yassar, High-entropy materials for lithium batteries, Batteries 10 (2024) 96.

[19] J.-W. Yeh, S.-K. Chen, S.-J. Lin, J.-Y. Gan, T.-S. Chin, T.-T. Shun, C.-H. Tsau, S.-Y. Chang, Nanostructured high-entropy alloys with multiple principal elements: novel alloy design concepts and outcomes, Adv. Eng. Mater. 6 (2004) 299–303.

[20] Y.F. Ye, Q. Wang, J. Lu, C.T. Liu, Y. Yang, The generalized thermodynamic rule for phase selection in multicomponent alloys, Intermetallics 59 (2015) 75–80.

[21] A. Sarkar, L. Velasco, D. Wang, Q. Wang, G. Talasila, L. de Biasi, C. Kübel, T. Brezesinski, S.S. Bhattacharya, H. Hahn, B. Breitung, High entropy oxides for reversible energy storage, Nat. Commun. 9 (2018) 3400.

[22] E.M. Kim, Y.Y. Li, B. Jin, S.M. Jeong, Innovative approaches to utilizing high-entropy oxide materials in lithium-ion batteries, Small 21 (2025) 2503776.

[23] G.K. S, T. Tomai, G. Halligudra, Y.N. S, C. Bekal, N.H. P, S. Kulkarni, K.G. R, S. C, M. Shetty, Insight into high-entropy oxides as anodes, cathodes, and solid-state electrolytes for advancing Li-ion batteries: a comprehensive review, J. Energy Storage 153 (2026) 120888.

[24] J. Su, Z. Cao, Z. Jiang, G. Chen, Y. Zhu, L. Wang, G. Li, High entropy oxide nanofiber by electrospun method and its application for lithium battery anode material, Int. J. Appl. Ceram. Technol. 19 (2022) 2004–2015.

[25] S. Chen, M. Bao, Y. Jia, X. Shao, Y. Guo, S. Li, A. Mao, J. Tan, X. Liu, Lattice distortion induced rock salt high-entropy oxide for high-rate lithium-ion storage, J. Alloys Compd. 990 (2024) 174480.

[26] C. Triolo, M. Maisuradze, M. Li, Y. Liu, A. Ponti, G. Pagot, V. Di Noto, G. Aquilanti, N. Pinna, M. Giorgetti, S. Santangelo, Charge storage mechanism in electrospun spinel-structured high-entropy $(Mn_{0.2}Fe_{0.2}Co_{0.2}Ni_{0.2}Zn_{0.2})_3O_4$ oxide nanofibers as anode material for Li-ion batteries, Small 19 (2023) 2304585.

[27] T.X. Nguyen, C.-C. Tsai, J. Patra, O. Clemens, J.-K. Chang, J.-M. Ting, Co-free high entropy spinel oxide anode with controlled morphology and crystallinity for outstanding charge/discharge performance in lithium-ion batteries, Chem. Eng. J. 430 (2022) 132658.

[28] M. Hodorová, D. Csík, A. Fedoročková, K. Gáborová, R. Džunda, G. Sučik, F. Kromka, K. Saksl, High-entropy perovskite $La(Co_{0.2}Mn_{0.2}Fe_{0.2}Ni_{0.2}Cu_{0.2})O_3$ as a material for lithium-ion batteries, Appl. Sci. 15 (2025) 10171.

[29] J. Yan, D. Wang, X. Zhang, J. Li, Q. Du, X. Liu, J. Zhang, X. Qi, A high-entropy perovskite titanate lithium-ion battery anode, J. Mater. Sci. 55 (2020) 6942–6951.

[30] X. Wang, Q. Liu, X. Wang, High-entropy materials: from bulk to sub-nano, Adv. Funct. Mater. 35 (2025) 2504275.

[31] Y. Wu, Z. Zhang, X. Jiang, Y. Zheng, Y. Zhao, Y. Ji, Z. Wang, X. Liu, Y. Zhang, S. Jiang, Research progress on high-entropy anode materials for alkali metal ion batteries, J. Energy Storage 148 (2026) 119955.

[32] O.F. Dippo, K.S. Vecchio, A universal configurational entropy metric for high-entropy materials, Scr. Mater. 201 (2021) 113974.

[33] X. Li, W. Zhang, K. Lv, J. Liu, A. Bayaguud, Research progress on high-entropy oxides as advanced anode, cathode, and solid-electrolyte materials for lithium-ion batteries, J. Power Sources 620 (2024) 235259.

[34] L. Dong, Y. Tian, C. Luo, W. Zhao, C. Qin, Z. Wang, Porous high-entropy oxide anode materials for Li-ion batteries: preparation, characterization, and applications, Materials 17 (2024) 1542.

[35] J. Yao, D. Wang, S. Liu, J. Zhang, W. Ding, C. Dong, High-entropy oxides anode: exploring the high-performance application from composition design to modification strategy in lithium ion battery, J. Energy Storage 146 (2026) 120192.

[36] S. Feng, H. Liu, Recent advances and understanding of high-entropy materials for lithium-ion batteries, Nanotechnology 35 (2024) 302001.

[37] J. Chen, X. Zhou, W. Wang, B. Liu, Y. Lv, W. Yang, D. Xu, Y. Liu, A review on fundamental of high entropy alloys with promising high–temperature properties, J. Alloys Compd. 760 (2018) 15–30.

[38] C. Qiu, Y. Li, X. Zhao, X. Kong, M. Guo, Z. Fang, Y. Zhao, Q. Sun, F. He, W. Li, Z. Liu, Progress on high-entropy oxide anode materials for advanced lithium-ion batteries, ChemSusChem 19 (2026) e202502653.

[39] F. Zhai, P. Yang, W. Zhang, X. Zhu, G. Cao, H. Zhang, Y. Xing, Y. Lei, Y. Xiang, S. Zhang, Creative high-entropy strategy: a booster to the design of anode materials for high-energy lithium-ion batteries, Rare Met. 44 (2025) 5907–5932.

[40] X. Xu, W. Li, W. Wang, N. Zhu, C. Tan, X. Gao, Y. Chen, High-entropy alloys for cathode, electrolyte, and anode applications in lithium-O_2 batteries, Batter. Supercaps 9 (2026) e70117.

[41] S. Sur, G. Anand, S.K. Jha, High entropy oxides for reversible lithium-ion battery: a brief review, Mater. Res. Express 11 (2024) 072003.

[42] X. Liu, Y. Xing, K. Xu, H. Zhang, M. Gong, Q. Jia, S. Zhang, W. Lei, Kinetically accelerated lithium storage in high-entropy (LiMgCoNiCuZn)O enabled by oxygen vacancies, Small 18 (2022) 2200524.

[43] K. Hou, X. Chang, X. Li, L. Wang, G. Liang, Carbon quantum dots modified amorphous-dominated high-entropy oxide $(FeCoNiCrMn)_3O_4$ as high-performance anodes for lithium ions storage, Ionics 32 (2026) 6977.

[44] X.L. Wang, E.M. Jin, G. Sahoo, S.M. Jeong, High-entropy metal oxide $(NiMnCrCoFe)_3O_4$ anode materials with controlled morphology for high-performance lithium-ion batteries, Batteries 9 (2023) 147.

[45] X. Guo, P. Gu, J. Wu, K. Li, Y. Liang, G. Wang, Z. Zhang, C. Guo, A novel Co-free high-entropy oxide $(FeNiCrMnMgAl)_3O_4$ as advanced anode material for lithium-ion batteries, J. Electroanal. Chem. 978 (2025) 118910.

[46] E. Lökçü, Ç. Toparli, M. Anik, Electrochemical performance of $(MgCoNiZn)_{1-x}Li_xO$ high-entropy oxides in lithium-ion batteries, ACS Appl. Mater. Interfaces 12 (2020) 23860–23866.

[47] P.M. Pratheeksha, S. Sivakanali, S.J. Kashyap, G. Chandra, D.P. Joseph, R. Vijay, T.N. Rao, S. Anandan, Effective oxygen-deficient $Li_4Ti_5O_{12}$ anode material displaying excellent rate performance and outstanding cyclic stability, ChemistrySelect 9 (2024) e202403479.

[48] Y. Li, Q. Li, J. Chai, Y. Wang, J. Du, Z. Chen, Y. Rui, L. Jiang, B. Tang, Si-based anode lithium-ion batteries: a comprehensive review of recent progress, ACS Mater. Lett. 5 (2023) 2948–2970.

[49] X. Yin, X. Li, P. lv, Z. Liu, H. Li, L. Bi, M. Qi, X. Mu, D. Guo, Smart construction of polyaniline shell on Fe_2O_3 as enabling high performance anode toward flexible lithium-ion battery, J. Mater. Sci. 59 (2024) 20686–20702.

[50] C. Hou, B. Wang, V. Murugadoss, S. Vupputuri, Y. Chao, Z. Guo, C. Wang, W. Du, Recent advances in Co_3O_4 as anode materials for high-performance lithium-ion batteries, Eng. Sci. 11 (2020) 19–30.

[51] S. Hao, B. Zhang, J. Feng, Y. Liu, S. Ball, J. Pan, M. Srinivasan, Y. Huang, Nanoscale ion intermixing induced activation of Fe_2O_3/MnO_2 composites for application in lithium ion batteries, J. Mater. Chem. A 5 (2017) 8510–8518.

[52] A. Kraytsberg, Y. Ein-Eli, A critical review-promises and barriers of conversion electrodes for Li-ion batteries, J. Solid State Electrochem. 21 (2017) 1907–1923.

[53] H. Kim, D.I. Kim, W.-S. Yoon, Challenges and design strategies for conversion-based anode materials for lithium- and sodium-ion batteries, J. Electrochem. Sci. Technol. 13 (2021) 32–53.

[54] J. Wang, Y. Wang, X. Lu, J. Qian, C. Yang, I. Manke, H. Song, J. Liao, S. Wang, R. Chen, Ultra-sleek high entropy alloy tights: realizing superior cyclability for anode-free battery, Adv. Mater. 36 (2024) 2308257.

[55] J. Xu, K. Liu, T. Xue, X. Jiang, H. Wang, C. Zhang, T. Lyu, X. Xiao, J. Yao, F. Luo, S. Geng, M. Huang, Y. Miao, X. Lin, J. Lin, S. Li, D. Wang, Y. Zhuang, Z. Zheng, AlMnCoNiFe high-entropy alloy nanoparticles-embedded carbon cloth: structure stability and fast charging for lean/anode-free lithium metal batteries, Energy Storage Mater. 83 (2025) 104735.

[56] F. Hu, L. Chen, B. Liao, H. Guo, H. Wang, H. Cao, X. Ouyang, Bilayer interphase engineering enabling practical anode-free lithium metal batteries, Energy Storage Mater. 81 (2025) 104497.

[57] J. Wang, P. Yang, Y. Wang, S. Wang, High entropy alloy nanoparticles decorated carbon-based electrode as interfacial Li-ion localized accelerators for anode-free lithium metal batteries, Carbon 228 (2024) 119432.

[58] Y. Liu, X. Geng, M. Ma, X. Xu, L. Chen, R. Li, L. Li, S. Yang, H. Xiang, In-situ modified lithiophilic layer enriched with multi-alloys and LiF for stable lithium metal anode, J. Alloys Compd. 1049 (2025) 185398.

[59] L. Zheng, R. Lv, C. Luo, Y. Guo, M. Yang, K. Hu, K. Wang, L. Li, F. Wu, R. Chen, Amorphous high-entropy alloy interphase for stable lithium metal batteries, Adv. Energy Mater. 14 (2024) 2402042.

[60] Q. Jin, F. Han, L. Zhang, H. Song, L. Feng, L. Wu, X. Zhang, F. Li, Magneto-electrochemical synergistic lithiophilic high-entropy alloy enables durable lithium metal anode, Energy Storage Mater. 83 (2025) 104717.

[61] C. Xu, T. Zhao, K. Wang, T. Yu, W. Tang, L. Li, F. Wu, R. Chen, Machine learning assisted design of high-entropy alloy interphase layer for lithium metal batteries, Adv. Funct. Mater. 35 (2025) 2425487.

[62] M. Ge, C. Cao, G.M. Biesold, C.D. Sewell, S.-M. Hao, J. Huang, W. Zhang, Y. Lai, Z. Lin, Recent advances in silicon-based electrodes: from fundamental research toward practical applications, Adv. Mater. 33 (2021) 2004577.

[63] C.K. Chan, H. Peng, G. Liu, K. McIlwrath, X.F. Zhang, R.A. Huggins, Y. Cui, High-performance lithium battery anodes using silicon nanowires, Nat. Nanotechnol. 3 (2008) 31–35.

[64] Y. Su, X. Lei, W. Chen, Y. Su, H. Liu, S. Ren, R. Tong, Y. Lin, W. Jiang, X. Liu, D. Su, Y. Zhang, Si-based all-lithium-reactive high-entropy alloy for thin-film lithium-ion battery anode, Chem. Eng. J. 500 (2024) 157197.

[65] Z. Ding, W. Ma, Q. Hao, T. Jian, Y. Yang, L. Yang, H. Gao, X. Li, J. Ma, C. Xu, H. Liu, From bulky Si to porous medium entropy alloy: enabling highly efficient Li storage via the simultaneous reconstruction of microstructure and component, J. Alloys Compd. 995 (2024) 174722.

[66] J.-H. Park, B.G. Kim, J. Shin, J. Hyun, S.Y. Jeong, J.I. Lee, S. Yang, K.-H. Nam, Stabilizing silicon anodes via high-entropy alloying and hierarchical carbon encapsulation for high-performance lithium-ion batteries, Carbon Lett. 36 (2026) 1265–1277.

[67] J. Zhao, Z. Wei, N. Chen, F. Meng, R. Tian, Y. Zeng, F. Du, High-entropy alloy anodes for low-strain and high-volumetric lithium-ion storage at ambient and subzero temperatures, Energy Storage Mater. 65 (2024) 103127.

[68] S.-H. Lee, K.-Y. Kim, J.-R. Yoon, Binder- and conductive additive-free laser-induced graphene/$LiNi_{1/3}Mn_{1/3}Co_{1/3}O_2$ for advanced hybrid supercapacitors, NPG Asia Mater. 12 (2020) 28.

[69] Y. Jiang, J.-L. Yue, Q. Guo, Q. Xia, C. Zhou, T. Feng, J. Xu, H. Xia, Highly porous Mn_3O_4 micro/nanocuboids with in situ coated carbon as advanced anode material for lithium-ion batteries, Small 14 (2018) 1704296.

[70] C.M. Rost, E. Sachet, T. Borman, A. Moballegh, E.C. Dickey, D. Hou, J.L. Jones, S. Curtarolo, J.-P. Maria, Entropy-stabilized oxides, Nat. Commun. 6 (2015) 8485.

[71] D. Wang, X. Li, T. Gu, Y. Li, X. Wen, Q. Wang, Y. Liu, X. Qi, Z. Wang, Manipulating lithium-ion storage behavior of high entropy oxide $(FeCoNiCrMn)_3O_4$ by tuning crystallinity, Powder Technol. 457 (2025) 120910.

[72] Y. Li, B. Wang, Y. Wang, R. Zheng, Z. Song, Z. Wang, Y. Liu, D. Wang, Modulating crystal structure and lithium-ion storage performance of high-entropy oxide $(CrMnFeCoNiZn)_3O_4$ by single element extraction, Composites, Part B Eng. 294 (2025) 112175.

[73] Y. Zheng, X. Wu, X. Lan, R. Hu, A spinel $(FeNiCrMnMgAl)_3O_4$ high entropy oxide as a cycling stable anode material for Li-ion batteries, Processes 10 (2021) 49.

[74] C. Liu, J. Bi, L. Xie, X. Gao, L. Meng, Preparation and electrochemical properties of two novel high entropy spinel oxides $(MgTiZnNiFe)_3O_4$ and $(CoTiZnNiFe)_3O_4$ by solid state reaction, Mater. Today Commun. 35 (2023) 106315.

[75] M.R. Esmaeili, S. Noorsina, S.K. Sadrnezhaad, High-entropy spinel-structured $(VCrNiCoMn)_3O_4$ anode for Li-ion batteries, J. Energy Storage 105 (2025) 114796.

[76] C. Duan, K. Tian, X. Li, D. Wang, H. Sun, R. Zheng, Z. Wang, Y. Liu, New spinel high-entropy oxides $(FeCoNiCrMnXLi)_3O_4$ (X = Cu, Mg, Zn) as the anode material for lithium-ion batteries, Ceram. Int. 47 (2021) 32025–32032.

[77] M. Możdżierz, J. Dąbrowa, A. Stępień, M. Zajusz, M. Stygar, W. Zając, M. Danielewski, K. Świerczek, Mixed ionic-electronic transport in the high-entropy $(Co,Cu,Mg,Ni,Zn)_{1-x}Li_xO$ oxides, Acta Mater. 208 (2021) 116735.

[78] J. Hao, J. Wang, W. Zhang, X. Li, Z. Xu, H. Liu, H. Wuliji, A. Bayaguud, Elevating oxygen vacancy of Co-free high-entropy oxide anode by lithium doping enables long-cycle lithium-ion batteries, J. Power Sources 669 (2026) 239372.

[79] C. Che, J. Bi, X. Zhang, Y. Yang, H. Wang, J. Rong, Synthesis and electrochemical performance of novel high-entropy spinel oxide $(FeCoMgCrLi)_3O_4$, J. Electroanal. Chem. 974 (2024) 118719.

[80] O.A. Podgornova, N.V. Kosova, Multi-anionic and multi-cationic high-entropy oxides as electrode materials for lithium-ion batteries, J. Power Sources 633 (2025) 236463.

[81] D. Wang, S. Jiang, C. Duan, J. Mao, Y. Dong, K. Dong, Z. Wang, S. Luo, Y. Liu, X. Qi, Spinel-structured high entropy oxide $(FeCoNiCrMn)_3O_4$ as anode towards superior lithium storage performance, J. Alloys Compd. 844 (2020) 156158.

[82] B. Xiao, G. Wu, T. Wang, Z. Wei, Y. Sui, B. Shen, J. Qi, F. Wei, J. Zheng, High-entropy oxides as advanced anode materials for long-life lithium-ion batteries, Nano Energy 95 (2022) 106962.

[83] J. Patra, T.X. Nguyen, A. Panda, C.-T. Hsieh, F.-M. Wang, T.-Y. Wu, C.-C. Yang, D. Bresser, J.-M. Ting, J.-K. Chang, Yolk-shell-structured $(CrMnFeCoNi)_3O_4$ high-entropy oxide anode for high-performance lithium-ion batteries, Electrochim. Acta 533 (2025) 146545.

[84] G. Jin, C. Luo, Z. Wang, S. Jia, H. Yu, C. Zhang, Q. Wang, B. Zhang, Z. Wang, Unraveling phase transition pathway of spinel $(FeCoCrNiMn)_3O_4$ high-entropy oxide anodes for long-life Li-ion batteries, Mater. Today Chem. 48 (2025) 102949.

[85] W. Song, D. Liu, B. Zhu, Y. He, S. Dou, X. Huang, M. Li, B. Zhong, Entropy-induced high-density grain boundaries in Co-free high-entropy spinel oxides for highly reversible lithium storage, J. Colloid Interface Sci. 677 (2025) 795–803.

[86] L. Oroszová, D. Csík, G. Baranová, G. Bortel, R. Džunda, L. Temleitner, M. Hagarová, B. Breitung, K. Saksl, Utilizing high-capacity spinel-structured high-entropy oxide $(CrMnFeCoCu)_3O_4$ as a graphite alternative in lithium-ion batteries, Crystals 14 (2024) 218.

[87] K. Tian, C. Duan, Q. Ma, X. Li, Z. Wang, H. Sun, S. Luo, D. Wang, Y. Liu, High-entropy chemistry stabilizing spinel oxide $(CoNiZnXMnLi)_3O_4$ (X = Fe, Cr) for high-performance anode of Li-ion batteries, Rare Met. 41 (2022) 1265–1275.

[88] Ext K. Wang, D. Wu, Y. Wei, L. Zhong, C. Wu, L. Song, B. Ge, Understanding the lithium storage mechanism of mesoporous structured high-entropy metal oxide anode with in situ transmission electron microscope, ACS Nano 19 (2025) 31457–31466.

[89] D. Csík, G. Baranová, R. Džunda, D. Zalka, B. Breitung, M. Hagarová, K. Saksl, High-entropy composite coating based on AlCrFeCoNi as an anode material for Li-ion batteries, Coatings 13 (2023) 1219.

[90] C. Che, J. Bi, X. Zhang, Y. Yang, H. Wang, J. Rong, Novel high-entropy oxide achieves high capacity and stability as an anode for lithium-ion batteries, Mater. Lett. 378 (2025) 137521.

[91] M. Zhao, X. Zhang, H. Yu, Y. Xie, T. Yi, Microscopic insight of the high-entropy effect on the lithium storage performance and rate capability of spinel oxide, Energy Environ. Mater. 8 (2025) e70060.

[92] Q. An, S. Li, J. Zhou, S. Ji, Z. Wen, J. Sun, Novel spinel multicomponent high-entropy oxide as anode for lithium-ion batteries with excellent electrochemical performance, Adv. Eng. Mater. 25 (2023) 2300585.

[93] C. Jin, Y. Wang, H. Dong, Y. Wei, R. Nan, Z. Jian, Z. Yang, Q. Ding, A novel spinel high-entropy oxide $(Cr_{0.2}Mn_{0.2}Co_{0.2}Ni_{0.2}Zn_{0.2})_3O_4$ as anode material for lithium-ion batteries, Inorganics 12 (2024) 198.

[94] X.L. Wang, E.M. Kim, T.G. Senthamaraikannan, D.-H. Lim, S.M. Jeong, Porous hollow high entropy metal oxides $(NiCoCuFeMg)_3O_4$ nanofiber anode for high-performance lithium-ion batteries, Chem. Eng. J. 484 (2024) 149509.

[95] C. Jin, M. Yuan, D. Tian, J. Jian, Y. Wei, R. Nan, Z. Yang, Q. Ding, Synthesis and lithium storage properties of spinel $(Al_{0.2}Mn_{0.2}Co_{0.2}Ni_{0.2}Zn_{0.2})_3O_4$ high-entropy oxide, Inorganics 14 (2025) 1.

[96] N. Qiu, H. Chen, Z. Yang, S. Sun, Y. Wang, Y. Cui, A high entropy oxide $(Mg_{0.2}Co_{0.2}Ni_{0.2}Cu_{0.2}Zn0.2O)$ with superior lithium storage performance, J. Alloys Compd. 777 (2019) 767–774.

[97] Z. Yang, X. Xiang, J. Yang, Z.-Y. Zhao, High-entropy oxides as energy materials: from complexity to rational design, Mater. Futur. 3 (2024) 042001.

[98] C. Zhang, M. Su, Y. Luo, X. Zhang, S. Li, F. Gao, Q. Lu, High entropy oxide duplex yolk–shell structure with isogenic amorphous/crystalline heterophase as a promising anode material for lithium-ion batteries, Small 21 (2025) 2407361.

[99] X. Liu, Y. Yu, K. Li, Y. Li, X. Li, Z. Yuan, H. Li, H. Zhang, M. Gong, W. Xia, Y. Deng, W. Lei, Intergrating hollow multishelled structure and high entropy engineering toward enhanced mechano-electrochemical properties in lithium battery, Adv. Mater. 36 (2024) 2312583.

[100] M. Zhao, H. Yu, Y. Xie, T. Yi, Integrating morphology modulation and high entropy engineering to unlock excellent lithium storage performance, Ceram. Int. 51 (2025) 13968–13979.

[101] H. Xu, R. Wang, F. Dong, Z. Yang, D. Li, Y. Xu, H. Ge, M. Yuan, Q. Kang, Structural engineering and high entropy effect toward improved mechano-electrochemical performance in lithium batteries, Rare Met. 44 (2025) 6040–6052.

[102] S. Gao, H. He, F. Zhai, W. Zhang, G. Cao, H. Zhang, J. Qiu, X. Zhu, F. Ding, Y. Xiang, Hollow graphene microsphere in situ deposited with rock-salt-type high-entropy oxide nanoparticles for enhanced rate performance as anodes in lithium-ion batteries, ACS Appl. Energy Mater. 8 (2025) 1896–1907.

[103] P. Ghigna, L. Airoldi, M. Fracchia, D. Callegari, U. Anselmi-Tamburini, P. D'Angelo, N. Pianta, R. Ruffo, G. Cibin, D.O. De Souza, E. Quartarone, Lithiation mechanism in high-entropy oxides as anode materials for Li-ion batteries: an operando XAS study, ACS Appl. Mater. Interfaces 12 (2020) 50344–50354.

[104] X. Chen, Y. Xiang, C. Li, S. Song, X. Liu, B. Luo, Y. Xiang, Co-stabilization of high-entropy oxides by entropy and polyanionic units toward high-capacity zero-strain anodes for advanced lithium-ion batteries, Adv. Sci. 13 (2026) e16795.

[105] L. Zhou, D. Zhao, X.W. Lou, Double-shelled $CoMn_2O_4$ hollow microcubes as high-capacity anodes for lithium-ion batteries, Adv. Mater. 24 (2012) 745–748.

[106] J. Hong, Z. Wang, W. Chen, L.-Y. Wang, C. Qu, Online joint-prediction of multi-forward-step battery SOC using LSTM neural networks and multiple linear regression for real-world electric vehicles, J. Energy Storage 30 (2020) 101459.

[107] G. Heyer, M. D'Arpino, G. Rizzoni, Performance metrics for the comparison of lithium ion cell aging experiments, Energy Rev. 2 (2023) 100025.

[108] J. Tian, Y. Fan, T. Pan, X. Zhang, J. Yin, Q. Zhang, A critical review on inconsistency mechanism, evaluation methods and improvement measures for lithium-ion battery energy storage systems, Renew. Sustain. Energy Rev. 189 (2024) 113978.

[109] B. Dong, M. Li, C. Yang, Z. Liang, Y. Guo, Z. Xing, M. Chen, K. Zhang, L. Zhou, Prelithiation of lithium-ion batteries towards commercialization: concepts, challenges, and application prospects, J. Mater. Chem. A 13 (2025) 15302–15327.

[110] L. Jin, C. Shen, Q. Wu, A. Shellikeri, J. Zheng, C. Zhang, J.P. Zheng, Pre-lithiation strategies for next-generation practical lithium-ion batteries, Adv. Sci. 8 (2021) 2005031.
[111] Z. Huang, Z. Deng, Y. Zhong, M. Xu, S. Li, X. Liu, Y. Zhou, K. Huang, Y. Shen, Y. Huang, Progress and challenges of prelithiation technology for lithium-ion battery, Carbon Energy 4 (2022) 1107–1132.
[112] Y. Luo, C. Zhang, M. Su, F. Zhen, S. Li, C. Wang, F. Gao, Q. Lu, Architecting high-entropy yolk–shell chalcogenide nanoarchitectures toward high-performance energy storage, Nano Res. 18 (2024) 94907510.
[113] W. Cheng, J. Liu, J. Hu, W. Peng, G. Niu, J. Li, Y. Cheng, X. Feng, L. Fang, M. Wang, S.A.T. Redfern, M. Tang, G. Wang, H. Gou, Pressure-stabilized high-entropy (FeCoNiCuRu)S_2 sulfide anode toward simultaneously fast and durable lithium/sodium ion storage, Small 19 (2023) 2301915.
[114] J. Shu, Y. Si, X. Ma, W. Lei, Y. Zhao, C. Shan, High entropy metal sulfide stabilized by ZIF-8-derived carbon as high-performance anode in lithium ion battery, Carbon 238 (2025) 120166.
[115] S. Alvi, A.P. Black, I. Jozami, C. Escudero, F. Akhtar, P. Johansson, Entropy stabilized medium high entropy alloy anodes for lithium-ion batteries, Batter. Supercaps 7 (2024) e202300585.
[116] R. Liu, J. Xue, W. Liu, F. Liang, J. Sun, S. Jia, Y. Gu, H. Zhao, Y. Yang, Q. Zou, Y. Yao, R. Tian, S. Wang, Nanostructured high-entropy sulfide interface engineering for accelerated Li+ kinetics in anode-free lithium metal batteries, Sci. China Chem. 69 (2026) 2073–2081.
[117] X. Lei, Y. Wang, J. Wang, Y. Su, P. Ji, X. Liu, S. Guo, X. Wang, Q. Hu, L. Gu, Y. Zhang, R. Yang, G. Zhou, D. Su, Si-based high-entropy anode for lithium-ion batteries, Small Methods 8 (2024) 2300754.
[118] L. Liu, X. Liu, J. Zhu, Z. Huo, B. Chen, W. Liang, M. Li, F. Lin, M. Zhao, D. Li, D. Chen, Z. Wang, P. Zhang, X. Lu, Y. Chen, L. Zhang, Y. Liu, Y. Wei, Rational design of high entropy metal phosphide anode for highly reversible lithium storage, Chem. Eng. J. 530 (2026) 173674.
[119] J. Du, X. Shen, B. Jin, L. Liao, Z. Mei, Q. Du, L. Liang, X. Tao, Hierarchical 3D honeycomb-inspired nanoarchitecture integrating silicon nanoparticles with high-entropy alloy matrix for ultrahigh-capacity lithium-ion battery anodes, J. Alloys Compd. 1053 (2026) 186157.
[120] F. Zhang, J. Zhao, G. Cai, H. Zhao, High-entropy NiCoFeMnCrP as anode materials for high-performance lithium-ion batteries, J. Phys. Chem. Solid. 208 (2026) 113161.
[121] Y. Wei, X. Liu, R. Yao, J. Qian, Y. Yin, D. Li, Y. Chen, Embedding the high entropy alloy nanoparticles into carbon matrix toward high performance Li-ion batteries, J. Alloys Compd. 938 (2023) 168610.
[122] W. Xiao, H. Xu, Y. Pei, L. Hu, Z. Yang, High entropy alloy/graphite composite as a new strategy to enhance the performance of lithium-ion batteries, SSRN Electron. J. (2024) 4961497.
[123] J. Wang, J. Jiang, P.K. Liaw, Y. Zhang, Properties and performances of high-entropy materials in batteries, Int. J. Miner. Metall. Mater. 32 (2025) 2786–2805.
[124] T. Xu, H. Feng, W. Liu, Y. Wang, H. Zheng, Opportunities and challenges of high-entropy materials in lithium-ion batteries, Rare Met. 43 (2024) 4884–4902.